Matrix Product State Simulations of Spin Chains at Finite Temperatures using State Purification

Matthijs Ates

Bachelor Thesis for Applied Physics & Applied Mathematics

June 2022

Student number:	5077990	
Thesis Committee:	Prof. Dr. J. Thijssen	Physics Supervisor
	Dr. N. Budko	Mathematics Supervisor
	Dr. A. Otte	
	Dr. J. Dubbeldam	

TU Delft

Abstract

The aim of this thesis is to simulate quantum spin chains at a finite temperature. This has been achieved by using purification to write the incoherent thermal states of the spin chain as pure states, after which the matrix product state (MPS) formalism to simulate the spin chain. The influence of temperature on the spin chain has been tested by comparing chain magnetization to the strength of the external magnetic field at different temperatures. Real time evolution has also been applied under the assumption that the time evolution is adiabatic. The results have been compared to the analytical solution found by directly calculating the density matrix. The model is very accurate for imaginary time evolution, which is required to evolve the system to the desired temperature. During real time evolution the results oscillate slightly around the analytical solution, which remains constant. This oscillation is a consequence of model truncation and the Suzuki-Trotter approximation. The effect of allocating more numerical resources to limit this phenomenon is explored, and a method to increase reachable timescales by decreasing entanglement growth in the chain over time is tested and verified.

Contents

1 Introduction

Many-body quantum systems have long been an object of study for physicists as they pose some of the most difficult challenges in physics, which are more often than not impossible to solve analytically. Computers have often been the saving grace for physicists and mathematicians due to their ability to rapidly perform calculations, which enables them to find solutions numerically. However, the complexity of quantum many-body systems grows exponentially with the number of particles in the system due to entanglement, and even computers have their limits. This has required physicists and mathematicians to come up with clever ways to describe quantum systems rather than using a brute-force approach, restricting to specific situations and approximating when necessary. Nevertheless, even when restricting to 1-dimensional lattices, the system size is a very limiting factor for standard computer algorithms.

In the beginning of the 1990s a new method to study such systems near the ground state was developed by Steven White[1], called the Density Matrix Renormalization Group (DMRG) algorithm. This method proved vastly superior to other existing methods at the time and quickly rose in popularity. Some years later a 'new generation' of DMRG arose, the Matrix Product State (MPS) method. Matrix product states already existed at the time White published his original paper. However, it took some years before its relationship to DMRG was recognized and adopted by researchers. Once this happened, researchers made swift progress extending the model to (among many other topics) time evolution[2], the application of periodic boundary conditions[3] and the extension of matrix product states to the operator space: matrix product operators[4].

Matrix product state algorithms have proven to be able to accurately simulate real world situations. For example, see the thesis work of J. Bouwmeester [5], which makes use of matrix product states to simulate the dynamics of a spin chain subject to excitations induced by a Scanning Tunneling Microscope and was thereby able to replicate the experimental results obtained at the Otte lab at the TU Delft department of Quantum Nanoscience [6].

In ref. [4] systems at finite temperature were simulated within the framework of matrix product states for the first time. The main difficulty that had to be overcome, was the fact that finite temperature mixed states are characterised by density operators instead of vectors and are therefore not suited to be written in MPS form. This was solved by the use of a process called purification, which holds that a mixed state is written as a pure state in a larger Hilbert space through the use of an auxiliary system. In this thesis we will use this approach to simulate spin chains governed by an XY-Hamiltonian with a transverse magnetic field at finite temperatures.

This research is a follow-up on the works of A. Melo, P. Vree and J. Bouwmeester, in which matrix product states were used to study different situations at zero temperature. In this research this model is extended to simulate spin chains at finite temperatures. The thesis is structured as follows: chapter 2 develops a mathematical basis for many-spin systems and discusses the Hamiltonian used during simulations. Chapter 3 introduces the notion of matrix product states and chapter 4 develops the theory of finite temperature systems, purification and their incorporation in the frame of MPS. The results are presented in chapter 5 and the thesis finishes with a summary and conclusion in chapter 6.

2 Quantum Mechanics and Spin Chains

2.1 Quantum States and Many Body Systems

In this section a few core concepts of quantum mechanics crucial to this research are summarized. Topics include the definition of spin states and how they are described mathematically, systems of multiple spin particles and spin chains. This is followed with a section regarding the Hamiltonian of the simulated spin chain. The chapter concludes with a short introduction on the graphical notation of tensors.

We will begin by examining the way a single quantum spin is described mathematically. A quantum spin is characterized by two quantum numbers, written together as the *ket* $|s\ m_s\rangle$, where s is a positive (half-)integer number called the *spin number* and $m_s \in \{-s,\ -s+1,\ \dots, s-1, s\}$ the z-component of the spin. Thus for a particle with spin number s there are a total of $(2s+1) \equiv d$ possible combinations $|s\ m_s\rangle$. To each $|s\ m_s\rangle$ state an orthonormal basis vector in a $(2s+1)$-dimensional complex vector space can be assigned. These basis vectors we denote $|n\rangle$, where $n = m_s + s + 1$. The spin can be in any complex linear combination of these basis vectors, provided it is *normalized* under the Euclidean norm.

Formally: the spin exists in the vector space $\{\underline{a} \mid \underline{a} \in \mathbb{C}^{(2s+1)} \ \wedge\ \langle \underline{a}|\underline{a}\rangle = 1\}$ equipped with inner product $\langle \underline{a}|\underline{b}\rangle \equiv \underline{a}^\dagger \underline{b}$, where $\dagger$ denotes the Hermitian conjugate. This vector space is complete, making it a *Hilbert space* we will denote as $\mathcal{H}$. The quantum state vector of the spin we then denote as the ket $|\psi\rangle$:

$$|\psi\rangle = \sum_{n=1}^{2s+1\equiv d} \alpha_n |n\rangle \qquad |\psi\rangle \in \mathcal{H}. \tag{1}$$

The Hermitian conjugate of the ket is called the *bra*: $|\psi\rangle^\dagger = \langle\psi|$. As previously stated all valid quantum states are normalized: $\langle\psi|\psi\rangle = 1$.

As an example we will look at a particle with $s = \frac{1}{2}$. Then $m_s \in \{\frac{1}{2},\ -\frac{1}{2}\}$ meaning we work in a two dimensional vector space ($d = 2$). By convention the orthonormal basis consist of the standard unit vectors: $|n\rangle = \underline{e}_n$. Then

$$|\psi\rangle = \alpha_1 |1\rangle + \alpha_2 |2\rangle = \alpha_1 \begin{bmatrix} 1 \\ 0 \end{bmatrix} + \alpha_2 \begin{bmatrix} 0 \\ 1 \end{bmatrix}.$$

Suppose we have a particle with spin s. This particle is fully described by equation (1). Now a second, identical spin is introduced. It is possible to describe both spins with a single state vector by using the tensor product. To avoid ambiguity we will introduce a new index that corresponds to each spin.

$$|\psi_1\rangle = \sum_{n_1=1}^{d} \alpha_{n_1}^{[1]} |1_{n_1}\rangle \qquad |\psi_1\rangle \in \mathcal{H}_1$$

$$|\psi_2\rangle = \sum_{n_2=1}^{d} \alpha_{n_2}^{[2]} |2_{n_2}\rangle \qquad |\psi_2\rangle \in \mathcal{H}_2$$

These two spins together can be described as a single vector in a d^2-dimensional Hilbert space $\mathcal{H}$ by using the tensor product:

$$|\Psi\rangle = |\psi_1\rangle \otimes |\psi_2\rangle = \sum_{n_1=1}^{d} \sum_{n_2=1}^{d} \alpha_{n_1}^{[1]} \alpha_{n_2}^{[2]} |1_{n_1}\rangle \otimes |2_{n_2}\rangle, \tag{2}$$

$$|\Psi\rangle \in \mathcal{H} = \mathcal{H}_1 \otimes \mathcal{H}_2.$$

Equation (2) is often written in a shorter form by leaving out the tensor product and dropping the site-specific indices:

$$|\Psi\rangle = \sum_{n_1,n_2=1}^{d} \alpha_{n_1} \alpha_{n_2} |n_1 n_2\rangle \equiv \sum_{n_1,n_2=1}^{d} c_{n_1 n_2} |n_1 n_2\rangle. \tag{3}$$

The form of equation (3) can be generalized to an arbitrary number of spins L that can each be in d different states.

$$|\Psi\rangle = \sum_{n_1 n_2 \ldots n_L} c_{n_1 n_2 \ldots n_L} |n_1 n_2 \ldots n_L\rangle \qquad |\Psi\rangle \in \mathcal{H} = \bigotimes_{i=1}^{L} \mathcal{H}_i, \tag{4}$$

where the summation bounds are left out for readability.

Operators and the Hamiltonian

Operators are matrices that act on states, which are vectors, by matrix-vector multiplication: $\hat{O}|\psi\rangle$. The expectation value of an operator is found by multiplying this with the Hermitian conjugate of the state (the bra): $\langle\hat{O}\rangle = \langle\psi|\hat{O}|\psi\rangle$. One important operator is the *Hamiltonian* $\hat{H}$, which is the operator that describes the energy of the system. Moreover the Hamiltonian (which is always a Hermitian operator) determines what happens to a system over time following the *time dependent Schrödinger equation* (TDSE):

$$i\hbar\frac{\partial|\psi\rangle}{\partial t} = \hat{H}|\psi\rangle, \qquad \text{a PDE with solution:} \qquad |\psi(t)\rangle = e^{\frac{-i\hat{H}t}{\hbar}}|\psi(0)\rangle. \tag{5}$$

Here $\hbar$ is the reduced Planck constant, which we set equal to 1 from this point forward. We will see in chapter 4 that time evolution has a close relationship to simulating quantum systems at finite temperature.

2.2 Spin Chains and the XY-Hamiltonian

A spin chain is a system where spins are arranged in a 1-dimensional lattice, where each spin interacts with its nearest neighbors, meaning that the Hamiltonian is a sum of operators acting on two neighboring sites (with of course the added possibility of single-site terms). Interactions other than nearest-neighbor are possible but are not considered in this research.

In this research a spin chain of length L consisting of spin-$\frac{1}{2}$ particles with open boundary conditions will be simulated at finite temperatures. The systems is governed by an XY-Hamiltonian with a transverse magnetic field of strength h:

$$\hat{H}_{\mathrm{XY}} = J\Big(\sum_{i=1}^{L-1}(\hat{\sigma}_x^{[i,i+1]} + \hat{\sigma}_y^{[i,i+1]}) + \sum_{i=1}^{L} h\hat{\sigma}_z^{[i]}\Big), \tag{6}$$

where the upper indices inside square brackets indicate the site or sites the operator acts on:

$$\hat{\sigma}_{x,y,z}^{[i]} = \Big(\bigotimes_{k=1}^{i-1}\hat{\mathbb{I}}_{2\times2}\Big) \otimes \hat{\sigma}_{x,y,z} \otimes \Big(\bigotimes_{k=i+1}^{L}\hat{\mathbb{I}}_{2\times2}\Big); \qquad \hat{\sigma}_{x,y,z}^{[i,i+1]} = \Big(\bigotimes_{k=1}^{i-1}\hat{\mathbb{I}}_{2\times2}\Big) \otimes \hat{\sigma}_{x,y,z} \otimes \hat{\sigma}_{x,y,z} \otimes \Big(\bigotimes_{k=i+2}^{L}\hat{\mathbb{I}}_{2\times2}\Big)$$

and $\hat{\sigma}_{x,y,z}$ denote the *Pauli spin matrices* for the spin-$\frac{1}{2}$ particle

$$\hat{\sigma_x} = \begin{bmatrix} 0 & 1 \\ 1 & 0 \end{bmatrix} \qquad \hat{\sigma_y} = \begin{bmatrix} 0 & -i \\ i & 0 \end{bmatrix} \qquad \hat{\sigma_z} = \begin{bmatrix} 1 & 0 \\ 0 & -1 \end{bmatrix}.$$

J is a constant, which we set equal to 1. If $J > 0$ we have an antiferromagnetic coupling between nearest neighbours, if $J < 0$ the coupling is ferromagnetic [7].

The XY model features only nearest-neighbour interactions between spins and therefore it can be efficiently simulated by Matrix Product States as entanglement between sites far apart will decay rapidly. This will be elaborated upon in the next section. The XY model without a magnetic field has already been solved exactly in 1961 by Lieb et al. [8]. However, it is not the aim of this study to examine the XY model specifically but to simulate a spin chain at nonzero temperature with matrix product states. This model allows for easy comparison between the influence of different magnetic field strengths and nonzero temperatures on $\langle\hat{S}_z\rangle$.

2.3 Graphical Representation of Tensors

In this work we will make use of a graphical tensor notation (the penrose graphical notation) for clarification of concepts a number of times. In this section a short explanation will be given.

In the penrose notation a tensor with L indices is represented by a block (or any other shape) with L lines protruding from it. Direction and length of the lines is irrelevant. Two tensors that are multiplied along a certain axis are represented by two blocks that share a single line. For example see figure 1b, where a multiplication between two matrices is represented. The result of a matrix product is again a matrix, which can be seen from the two free lines that still extend from the combination of the two blocks. As a last note it should be mentioned that a block without any lines extending from it is a scalar, see figure 1c.

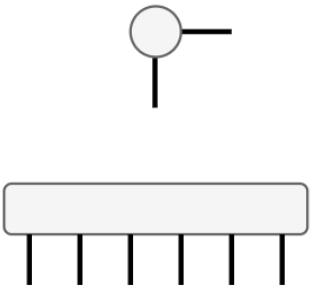

(a) Two tensors in graphical notation. The upper is a tensor of order 2 (a matrix), the lower a tensor of order 6.

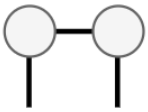

(b) Multiplication of two matrices.

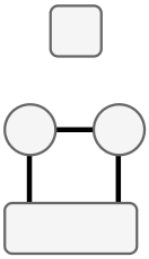

(c) Two examples of a scalar in tensor notation.

Figure 1: Examples of the graphical notation used to represent tensors and contractions in this thesis.

3 Matrix Product States

Singular Value Decomposition

Before examining matrix product states there is an important concept from linear algebra that needs to be discussed: the *Compact Singular Value Decomposition*, which we will from now on refer to as the Singular Value Decomposition (SVD). Given any matrix C of arbitrary dimensions $(n \times m)$ there exists a decomposition

$$C = U\Lambda V^\dagger, \tag{7}$$

where the columns of U are the *left singular vectors*, the rows of $V^\dagger$ are the *right singular vectors* and Λ is a diagonal matrix containing the *singular values*. If r denotes the number of nonzero singular values λ_r in Λ, then the dimensions of the matrices are: U $(n \times r)$, Λ $(r \times r)$ and $V^\dagger$ $(r \times m)$. Observe that there are an equal number of left and right singular vectors, but the left and right singular vectors are not necessarily of the same dimension. Moreover, the sets $\{\mathbf{u}_i\}$ and $\{\mathbf{v}_i\}$ of respectively the left and right singular vectors are orthonormal and the number r of nonzero singular values equals the rank of matrix C. Lastly, the singular values are chosen to be decreasing: $\Lambda_{1,1} \geq \Lambda_{2,2} \geq ... \geq \Lambda_{r,r}$. The proofs of these properties and the exact procedure to find the singular vectors and singular values is explained in detail in [9].

3.1 Schmidt Decomposition, Entropy and the Area Law

The matrix product states formalism finds its roots in the so called *Schmidt decomposition* [10], which we will later see is closely related to the singular value decomposition. Consider a 1-dimensional system, consisting of L d-level systems with nearest-neighbour interactions. The Hilbert space of the system we denote $\mathcal{H}$. Suppose at a certain location in the chain the system is partitioned into parts A and B where $A(B)$ contains all particles to the left (right) of the split. Similarly the Hilbert space is decomposed into parts A and B: $\mathcal{H} = \mathcal{H}_A \otimes \mathcal{H}_B$, where $\mathcal{H}_{A(B)}$ denotes the Hilbert space of all sites on the left (right) side. The Schmidt decomposition of a quantum state $|\psi\rangle \in \mathcal{H}$ is then given as:

$$|\psi\rangle = \sum_\alpha \lambda_\alpha |\alpha\rangle_A \otimes |\alpha\rangle_B , \qquad |\alpha\rangle_{A(B)} \in \mathcal{H}_{A(B)}. \tag{8}$$

The *Schmidt indices* λ_α are real, strictly positive, unique up to degeneracies and for a normalized state $|\psi\rangle$ we have $\sum_\alpha \lambda_\alpha^2 = 1$. Moreover, the $\{|\alpha\rangle_{A(B)}\}$ form an orthogonal basis for their respective Hilbert spaces. Observe that when only a single λ_α is nonzero we obtain $|\psi\rangle = |\alpha\rangle_A \otimes |\alpha\rangle_B$, meaning that $|\psi\rangle$ is a product state between the left and right sides of the location of the split. Likewise, if more than one λ_α is nonzero then $|\psi\rangle$ is an entangled state.

A measure of the entanglement between the left and right parts of the system is given by the *Von Neumann entropy*, which is defined as ($\hat{\rho} = |\psi\rangle\langle\psi|$):

$$S = -Tr(\hat{\rho}\log_2(\hat{\rho})). \tag{9}$$

In the case that the composite system AB is in a pure state, then $S(A) = S(B) = S$ [11]. With this assumption and by writing $|\psi\rangle$ as in (8) evaluating formula (9) yields [12]

$$S = -\sum_\alpha \lambda_\alpha^2 \log_2(\lambda_\alpha^2), \tag{10}$$

meaning all information regarding the entanglement between systems A and B is contained in the Schmidt indices λ_α. A product state has only a single nonzero Schmidt value, which has value 1. Therefore product states have entropy 0.

As a rule, for a general state in the Hilbert space $\mathcal{H}$ the entropy follows a volume law, meaning it scales linearly with the volume of the system, as is similar to classical statistical mechanics (where entropy is an extensive quantity). However in some situations this rule does not necessarily hold. For systems with local gapped Hamiltonians that are near the ground state, the entropy follows an area law instead. Seeing as a 1-dimensional system has a constant boundary this means that the entropy will also be constant. An intuitive explanation is given by the fact that at lower energies particles further away will be very lowly entangled, thus only particles close to the system split will entangle the two partitions, see also figure 2. A proof of this theorem is presented in [13]. It should be noted that the area law states make up but a small part of the total Hilbert space. A useful property of area law states (which we will make use of later) is that the Schmidt values quickly decrease due to low entanglement, only a few contribute significantly. Thus the Schmidt decomposition of an area law state can be described by a small number of Schmidt values with a relatively small error.

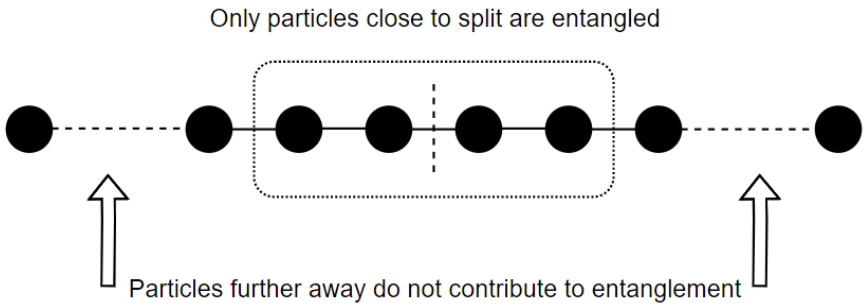

Figure 2: Visual motivation for the area law: only spins close to the system split (vertical dashed line) entangle the two systems while particles further away do not contribute to entanglement. Thus all particles more than a few sites away can be ignored and the system does not follow a volume law.

3.2 Matrix Product States

In this section we will develop the matrix product state formalism, which is the basis for most of this research. Matrix product states make use of the rapidly decaying Schmidt values of area law states to reduce the storage complexity of the system with minimal loss of information, and there exists an efficient time evolution algorithm (TEBD) based on the Suzuki-Trotter approximation that exploits the fact that the Hamiltonian only contains nearest-neighbor interaction. This makes matrix product states a powerful tool for analyzing spin chains with local Hamiltonians. This section is based on [5, 14].

We start with a general pure state $|\psi\rangle$ on a chain of L sites, with $\{|n_i\rangle\}$ a d-dimensional orthonormal basis for the local states at site i. The state can be written as in equation (4), repeated here for convenience

$$|\psi\rangle = \sum_{n_1 n_2 ... n_L} c_{n_1 n_2 ... n_L} |n_1 n_2 ... n_L\rangle \qquad |\psi\rangle \in \mathcal{H}.$$

Recall that $\mathcal{H}$ is the system Hilbert space and $|n_1 n_2 ... n_L\rangle = \bigotimes_{i=1}^{L} |n_i\rangle$.

It is our aim to write the coefficient $c_{n_1 n_2 ... n_L}$ as a product of matrices $A_{n_1} A_{n_2} ... A_{n_L}$ resulting in the *matrix product state* form:

$$|\psi\rangle = \sum_{n_1 n_2 ... n_L} A^{[1]}_{n_1} A^{[2]}_{n_2} ... A^{[L]}_{n_L} |n_1 n_2 ... n_L\rangle \,. \tag{11}$$

To ensure the product of the matrices results in a scalar coefficient, the first and last matrices ($A^{[1]}_{n_1}$ and $A^{[L]}_{n_L}$) are row and column vectors respectively. The upper indices indicate that each site in the chain has its own set of matrices. From this point on the upper indices will be dropped for readability.

To obtain the matrix product state we start by reshaping the d^L dimensional vector $c_{n_1 n_2 ... n_L}$ into a $d \times d^{L-1}$ dimensional matrix C and performing a singular value decomposition. Explicitly: we create a matrix C where $C_{n_1,\, n_2 ... n_L} = c_{n_1 n_2 ... n_L}$ and perform a singular value decomposition

$$C_{n_1,\, n_2 ... n_L} = \sum_{a_1=1}^{r_1} U_{n_1,\, a_1} \Lambda_{a_1,\, a_1} V^{\dagger}_{a_1,\, n_2 ... n_L}, \tag{12}$$

where a_1 is the *bond index* and r_1 the *bond dimension*. Observe that each row in U corresponds to a single value n_1. These d row vectors (of length $r_1 \leq d$) will be our A_{n_1} 'matrices'. Next, we reshape the $(r_1 \times d^{L-1})$ sized matrix $(\Lambda V^{\dagger})_{a_1,\, n_2 ... n_L}$ into a new matrix $C_{a_1 n_2,\, n_3 ... n_L}$ of size $(r_1 d \times d^{L-2})$ and perform another singular value decomposition:

$$C_{a_1 n_2,\, n_3 ... n_L} = \sum_{a_2}^{r_2} U_{a_1 n_2,\, a_2} \Lambda_{a_2,\, a_2} V^{\dagger}_{a_2,\, n_3 ... n_L}. \tag{13}$$

Again each $U_{a_1 n_2,\, a_2}$ corresponds to a single value of n_2, thus we get a set of d $(r_1 \times r_2)$ matrices A_{n_2} with $r_2 \leq d^2$. If we substitute equation (13) back into (12) we get:

$$c_{n_1 n_2 \ldots n_L} = C_{n_1 n_2,\, n_3 \ldots n_L} = \sum_{a_1=1}^{r_1} \sum_{a_2=2}^{r_2} A_{n_1,\, a_1} A_{n_2,\, a_1,\, a_2} \Lambda_{a_2,\, a_2} V^{\dagger}_{a_2,\, n_3 \ldots n_L}. \tag{14}$$

By continuing this process of contracting, reshaping and decomposing for each site in the chain we obtain the entire set of A_{n_i} matrices, with the last one (A_{n_L}) being a column vector. Upon completion we are left with:

$$c_{n_1 n_2 \ldots n_L} = \sum_{a_1 a_2 \ldots a_{L-1}} A_{n_1,\, a_1} A_{n_2,\, a_1,\, a_2} \ldots A_{n_L,\, a_{L-1}} \equiv A_{n_1} A_{n_2} \ldots A_{n_L}. \tag{15}$$

To finish the derivation we substitute this back into equation (4) and obtain equation (11).

An important detail we should pay attention to are the dimensions of the A_{n_i}, the previously mentioned bond dimensions. These originate from the singular value decomposition, thus by construction they are bounded to be $r_i \leq min\{d^i \times d^{L-i}\}$, increasing first and decreasing again after $i \geq \frac{L}{2}$, resulting in a row-vector product.

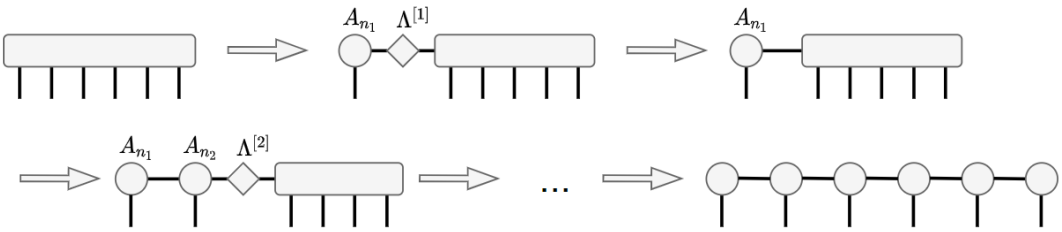

Figure 3: A graphical representation of the decomposition from a state where the coefficients are stored in a rank L tensor to a matrix product state by applying SVD's repeatedly.

To obtain a better understanding of what the consecutive singular value decompositions represent it is useful to examine how they relate to Schmidt decompositions. Suppose we want to find the Schmidt decomposition of $|\psi\rangle$ at site i. It is shown in [14] that performing SVD's from the left side of the chain up to site i and from the right side up to site $i+2$ we obtain a decomposition $c_{n_1 n_2 \ldots n_L} = \sum_{a_i}^{r_i} A_{n_1} \ldots A_{n_i,\, a_i} \Lambda_{a_i,\, a_i} B_{n_{i+1},\, a_i} B_{n_{i+2}} \ldots B_{n_L}$. Then we can introduce vectors

$$|a_i\rangle_A = \sum_{n_1 \ldots n_i} A_{n_1} \ldots A_{n_i} |n_1 \ldots n_i\rangle \qquad |a_i\rangle_B = \sum_{n_{i+1} \ldots n_L} B_{n_{i+1}} \ldots B_{n_L} |n_{i+1} \ldots n_L\rangle$$

and we obtain the Schmidt decomposition

$$|\psi\rangle = \sum_{a_i} \Lambda_{a_i,\, a_i} |a_i\rangle_A \otimes |a_i\rangle_B .$$

Note that the Schmidt values Λ_{a_i,a_i} are the singular values form the i-th singular value decomposition (and are therefore decreasing). In section 3.1 we discussed that area law states have rapidly decreasing Schmidt values, making it possible to discard many of them with little loss of information. This translates to the matrix product states formalism as truncating the A_{n_i} matrices. Say we want to keep the first χ Schmidt values, then all matrices A_{n_i} are truncated to be at most $(\chi \times \chi)$. The new bond dimensions are then $\tilde{r}_i \leq min\{d^i, d^{L-i}, \chi\}$. Doing so reduces the storage complexity of the system to be $\mathcal{O}(dL\chi^2)$ which scales *linearly* with system length instead of exponentially[15].

For the application of operators it is useful to write the MPS in the so called *canonical form* by inserting $\Lambda^{[i]}(\Lambda^{[i]})^{-1}$ between each A_{n_i} and $A_{n_{i+1}}$, resulting in equation (16).

$$|\psi\rangle = \sum_{n_1 n_2 \ldots n_L} \Gamma_{n_1} \Lambda^{[1]} \Gamma_{n_2} \ldots \Lambda^{[L-1]} \Gamma_{n_L} |n_1 n_2 \ldots n_L\rangle , \tag{16}$$

where $\Gamma_{n_i} = (\Lambda^{[i-1]})^{-1} A_{n_i}$ for $i > 1$ and $\Gamma_{n_1} = A_{n_1}$. We will use expression (16) for the application of operators, which is described in further detail in the next section. The canonical form is presented graphically in figure 4.

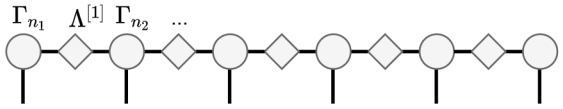

Figure 4: The tensor notation representation of the canonical form, as written in equation (16).

3.3 Application of Operators

An important aspect of quantum mechanics is the application of operators and the calculation of expectation values. The MPS formalism allows us to calculate these in an efficient way. The mathematical procedures for the application of single-site and two-site operators as well as an efficient method of calculating the inner product between two states are explained in this section. This section is based on previous works [5, 10, 15].

A useful consequence of the matrix product states formalism is the fact that the application of a single-site operator acting on site i ($\hat{O}^{[i]} = \hat{\mathbb{I}}^{[1]} \otimes ... \hat{\mathbb{I}}^{[i-1]} \otimes \hat{O} \otimes \hat{\mathbb{I}}^{[i+1]} ... \otimes \hat{\mathbb{I}}^{[L]}$) only affects the Γ_{n_i}, all other matrices remain the same. As a consequence all identity operators can be disregarded and we only need to focus on the application of $\hat{O}$ .To apply this operator we first perform two Schmidt decompositions: one between sites $i-1$ and i, and the other between sites i and $i+1$, resulting in the following description of our state:

$$|\psi\rangle = \sum_{n_i} \sum_{\alpha_{i-1}\alpha_i} \Lambda^{[i-1]}_{\alpha_{i-1}} \Gamma_{n_i} \Lambda^{[i]}_{\alpha_i} \left|a_{\alpha_{i-1}}\right\rangle_A |n_i\rangle |a_{\alpha_i}\rangle_B \equiv \sum_{n_i} \sum_{\alpha_{i-1}\alpha_i} \Theta^{\alpha_{i-1}\alpha_i}_{n_i} \left|a_{\alpha_{i-1}}\right\rangle_A |n_i\rangle |a_{\alpha_i}\rangle_B ,$$

where $\Lambda^{[i]}_j$ is used as shorthand for $\Lambda^{[i]}_{j,j}$. We now apply the operator $\hat{O}^{[i]}$ and insert the unit operator $\hat{\mathbb{I}} = \sum_{n'_i} |n'_i\rangle\langle n'_i|$:

$$\hat{O}^{[i]} |\psi\rangle = \sum_{n_i} \sum_{\alpha_{i-1}\alpha_i} \sum_{n'_i} \Theta^{\alpha_{i-1}\alpha_i}_{n_i} \langle n'_i| \hat{O}^{[i]} |n_i\rangle \left|a_{\alpha_{i-1}}\right\rangle_A |n'_i\rangle |a_{\alpha_i}\rangle_B = \sum_{\alpha_{i-1}\alpha_i} \sum_{n'_i} \tilde{\Theta}^{\alpha_{i-1}\alpha_i}_{n'_i} \left|a_{\alpha_{i-1}}\right\rangle_A |n'_i\rangle |a_{\alpha_i}\rangle_B , \tag{17}$$

where $\tilde{\Theta}^{\alpha_{i-1}\alpha_i}_{n'_i} \equiv \sum_{n_i} \Theta^{\alpha_{i-1}\alpha_i}_{n_i} \langle n'_i| \hat{O}^{[i]} |n_i\rangle$. In the last step we return to the canonical MPS form with the new matrices $\tilde{\Gamma}_{n_i}$:

$$\tilde{\Gamma}_{n_i} = (\Lambda^{[i-1]})^{-1} \tilde{\Theta}_{n'_i} (\Lambda^{[i]})^{-1}.$$

Thus in the end the application of a single-site operator on site i results in the change $\Gamma_{n_i} \to \tilde{\Gamma}_{n_i}$. This operation is of complexity $\mathcal{O}(d\chi^2)$.

A similar procedure can be done for a two-site operator $\hat{O}^{[i,i+1]}$ acting on site i and $i+1$. Again we perform two Schmidt decompositions, now resulting in

$$\begin{aligned} |\psi\rangle &= \sum_{n_i} \sum_{\alpha_{i-1}\alpha_i\alpha_{i+1}} \Lambda^{[i-1]}_{\alpha_{i-1}} \Gamma_{n_i} \Lambda^{[i]}_{\alpha_i} \Gamma_{n_{i+1}} \Lambda^{[i+1]}_{\alpha_{i+1}} \left|a_{\alpha_{i-1}}\right\rangle_A |n_i n_{i+1}\rangle |a_{\alpha_i+1}\rangle_B \\ &= \sum_{n_i} \sum_{\alpha_{i-1}\alpha_i\alpha_{i+1}} \Theta^{\alpha_{i-1}\alpha_{i+1}}_{n_i n_{i+1}} \left|a_{\alpha_{i-1}}\right\rangle_A |n_i n_{i+1}\rangle |a_{\alpha_i+1}\rangle_B . \end{aligned}$$

We apply the operator, insert $\mathbb{I} = \sum_{n'_i n'_{i+1}} \left|n'_i n'_{i+1}\right\rangle \left\langle n'_i n'_{i+1}\right|$ and define

$$\tilde{\Theta}^{n'_i n'_{i+1}}_{\alpha_{i-1}\alpha_{i+1}} \equiv \sum_{n_i n_{i+1}} \Theta^{\alpha_{i-1}\alpha_{i+1}}_{n_i n_{i+1}} \left\langle n'_i n'_{i+1}\right| \hat{O}^{[i,i+1]} |n_i n_{i+1}\rangle$$

as before. We then obtain

$$\hat{O}^{[i,i+1]} |\psi\rangle = \sum_{\alpha_{i-1}\alpha_{i+1}} \sum_{n'_i n'_{i+1}} \tilde{\Theta}^{\alpha_{i-1}\alpha_{i+1}}_{n'_i n'_{i+1}} \left|a_{\alpha_{i-1}}\right\rangle_A \left|n'_i n'_{i+1}\right\rangle |a_{\alpha_i+1}\rangle_B , \tag{18}$$

However, for the two-site operator there is a key difference from the procedure we had with the single-site operator. The state is still contracted between sites i and $i+1$, meaning we must reshape $\tilde{\Theta}$ into a matrix and perform an SVD to obtain the matrices for the individual sites

$$\tilde{\Theta}^{\alpha_{i-1}\alpha_{i+1}}_{n_i' n_{i+1}'} \to \tilde{\Theta}_{(n_i'\alpha_i-1),(n_{i+1}'\alpha_{i+1})} = U^{\alpha_{i-1}\alpha_i}_{n_i'} \tilde{\Lambda}^{[i]}_{\alpha_i} V^{\alpha_i\alpha_{i+1}}_{n_{i+1}'}. \tag{19}$$

Then lastly the updated matrices are defined as:

$$\begin{aligned} \Gamma_{n_i} &\to \tilde{\Gamma}_{n_i} = (\Lambda^{[i-1]})^{-1} U_{n_i} \\ \Lambda^{[i]} &\to \tilde{\Lambda}^{[i]} \\ \Gamma_{n_{i+1}} &\to \tilde{\Gamma}_{n_{i+1}} = V_{n_{i+1}} (\Lambda^{[i+1]})^{-1}. \end{aligned}$$

During this operation the size of the new $\tilde{\Gamma}$ and $\tilde{\Lambda}$ matrices may increase, however they can easily be truncated by discarding the lowest singular values, resulting in minimal loss of information. Normalization can be maintained by scaling the matrices. The application of the two-site operator is of complexity $\mathcal{O}(d^4\chi^2)$. The process of applying a two-site operator is visualised in figure 5.

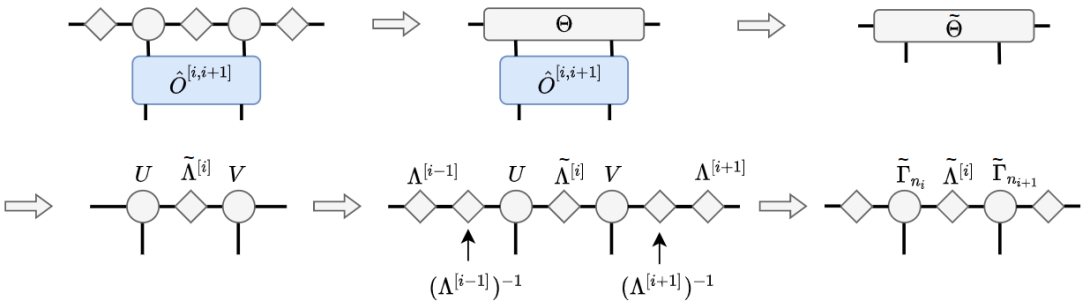

Figure 5: Application of a two-site operator.

The expectation values for single-site and two-site operators are given by [5]

$$\begin{aligned} \langle\psi|\,\hat{O}^{[i]}\,|\psi\rangle &= \sum_{\alpha_{i-1}\alpha_i} \sum_{n_i'} (\Theta^{\alpha_{i-1}\alpha_i}_{n_i'})^\dagger \tilde{\Theta}^{\alpha_{i-1}\alpha_i}_{n_i'} \\ \langle\psi|\,\hat{O}^{[i,i+1]}\,|\psi\rangle &= \sum_{\alpha_{i-1}\alpha_{i+1}} \sum_{n_i' n_{i+1}'} (\Theta^{\alpha_{i-1}\alpha_{i+1}}_{n_i' n_{i+1}'})^\dagger \tilde{\Theta}^{\alpha_{i-1}\alpha_{i+1}}_{n_i' n_{i+1}'}. \end{aligned}$$

The dot product between two quantum states $|\psi_i\rangle$ and $|\psi_2\rangle$ in MPS form can be calculated using the zip-up method[15]. This method scales polynomial with system length whereas calculating the dot product directly scales exponentially. The idea of the zip-up method is to start at one end of the chain and creating a matrix M_1. This matrix is used to calculate the next matrix M_2 and continuing this process through the chain. If we have states

$$\begin{aligned} |\psi\rangle &= \sum_{n_1 n_2 \ldots n_L} \Gamma_{n_1} \Lambda^{[1]} \Gamma_{n_2} \ldots \Lambda^{[L-1]} \Gamma_{n_L} |n_1 n_2 \ldots n_L\rangle \\ |\phi\rangle &= \sum_{n_1 n_2 \ldots n_L} \Omega_{n_1} K^{[1]} \Omega_{n_2} \ldots K^{[L-1]} \Omega_{n_L} |n_1 n_2 \ldots n_L\rangle, \end{aligned}$$

then we calculate $\langle\psi|\phi\rangle$ as follows:

$$\begin{aligned} M_1^{\alpha_1'\alpha_1} &= \sum_{n_1} (\Gamma^{\alpha_1'}_{n_1})^\dagger \Omega^{\alpha_1}_{n_1} (\Lambda^{[1]}_{\alpha_1'})^\dagger K^{[1]}_{\alpha_1} \\ M_2^{\alpha_2'\alpha_2} &= \sum_{n_2} \sum_{\alpha_1'\alpha_1} M_1^{\alpha_1'\alpha_1} (\Gamma^{\alpha_1',\alpha_2'}_{n_2})^\dagger K^{\alpha_1,\alpha_2}_{n_2} (\Lambda^{[2]}_{\alpha_2'})^\dagger \Omega^{[2]}_{\alpha_2}. \end{aligned}$$

The process continues until the end of the chain is reached. The number of calculations to calculate M_i scales with order $\mathcal{O}(d\chi^4)$.

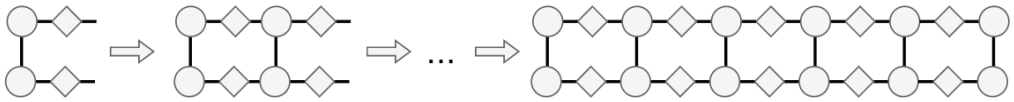

Figure 6: Graphical representation of the zip-up method for calculating the dot product.

3.4 Time Evolution of Matrix Product States

The time-dependent Schrödinger equation tells us that a quantum state $|\psi\rangle$ under Hamiltonian $\hat{H}$ evolves over time according to equation (5) repeated below ($\hbar = 1$)

$$|\psi(t)\rangle = e^{-i\hat{H}t}\,|\psi(0)\rangle\,.$$

In the previous section we have presented a way to efficiently apply single-site and two-site operators to a state in MPS form. If the Hamiltonian of a spin chain can be written in terms of such operators the system can be evolved through (imaginary) time in an efficient way using matrix product states. This idea is at the heart of the Time-Evolving Block Decimation algorithm, the focus of this section.

Suppose we have a Hamiltonian that we split into two parts: $\hat{H} = \hat{H}_A + \hat{H}_B$, so that we can write the Hamiltonian time evolution as $e^{-i\hat{H}t} = e^{-i(\hat{H}_A+\hat{H}_B)t} = e^{-i\hat{H}_A t}e^{-i\hat{H}_B t}$. If $\hat{H}_A$ and $\hat{H}_B$ commute this is possible, however when they do not commute this expression does not hold[16]. A problematic property of the consecutive nearest-neighbor coupling present in spin chains is that it is not possible to write the Hamiltonian in such a way that the two terms commute, and therefore we cannot write it in terms of two-site operators. The *Suzuki-Trotter approximation*[17] states that doing so will result in an error of $\mathcal{O}(t^2)$

$$e^{(\hat{A}+\hat{B})t} = e^{\hat{A}t}e^{\hat{B}t} + \mathcal{O}(t^2)\,; \qquad [\hat{A},\hat{B}] \neq 0. \tag{20}$$

Let us look at our Hamiltonian:

$$\hat{H}_{\mathrm{XY}} = J\Big(\sum_{i=1}^{L-1}(\hat{\sigma}_x^{[i,i+1]} + \hat{\sigma}_y^{[i,i+1]}) + \sum_{i=1}^{L} h\hat{\sigma}_z^{[i]}\Big) \equiv \sum_{i=1}^{L-1}\hat{K}^{[i,i+1]} + \sum_{i=1}^{L}\hat{K}^{[i]}.$$

We will split this Hamiltonian into two non-commuting parts $\hat{H}_{\mathrm{odd}}$ and $\hat{H}_{\mathrm{even}}$. The former contains all two-site operators where i is an odd number, the latter contains those where it is an even number. The single-site operators are split evenly between both parts, except for the last site, which is added to $\hat{H}_{\mathrm{odd}}$ is the chain is of even length and to $\hat{H}_{\mathrm{even}}$ if the chain is of odd length. For a chain of even length $\hat{H}_{\mathrm{odd}}$ and $\hat{H}_{\mathrm{even}}$ will therefore have the following form:

$$\begin{aligned}
\hat{H}_{\mathrm{odd}} &= \sum_{\substack{i=1\\ i\text{ odd}}}^{L-1} K^{[i,i+1]} + \frac{1}{2}\sum_{i=2}^{L-1}\hat{K}^{[i]} + \hat{K}^{[1]} \equiv \sum_{\substack{i=1\\ i\text{ odd}}}^{L-1}\hat{O}^{[i,i+1]} \\
\hat{H}_{\mathrm{even}} &= \sum_{\substack{i=1\\ i\text{ even}}}^{L-1} \hat{K}^{[i,i+1]} + \frac{1}{2}\sum_{i=2}^{L-1}\hat{K}^{[i]} + \hat{K}^{[L]} \equiv \sum_{\substack{i=1\\ i\text{ even}}}^{L-1}\hat{O}^{[i,i+1]} \\
\hat{H}_{\mathrm{XY}} &= \hat{H}_{\mathrm{odd}} + \hat{H}_{\mathrm{even}},
\end{aligned}$$

where we introduced the operators $\hat{O}^{[i,i+1]} = \hat{K}^{[i,i+1]} + \frac{1}{2}(\hat{K}^{[i]} + \hat{K}^{[i+1]})$. For completion $\frac{1}{2}\hat{K}^{[1]}$ and $\frac{1}{2}\hat{K}^{[L]}$ are added to $\hat{O}^{[1,2]}$ and $\hat{O}^{[L-1,L]}$ respectively. It is clear that $\hat{H}_{\mathrm{odd}}$ and $\hat{H}_{\mathrm{even}}$ do not commute with each other, however all terms inside $\hat{H}_{\mathrm{odd}}$ and $\hat{H}_{\mathrm{even}}$ are mutually commuting. That is to say: all terms in $\hat{H}_{\mathrm{odd}}$ ($\hat{H}_{\mathrm{even}}$) commute with all other terms in $\hat{H}_{\mathrm{odd}}$ ($\hat{H}_{\mathrm{even}}$). Therefore the exponents involving them can be decomposed exactly:

$$e^{-i\hat{H}_{\text{odd}}t} = \prod_{\substack{i=1 \\ i \text{ odd}}}^{L-1} e^{-i\hat{O}^{[i,i+1]}t}$$
$$e^{-i\hat{H}_{\text{even}}t} = \prod_{\substack{i=1 \\ i \text{ even}}}^{L-1} e^{-i\hat{O}^{[i,i+1]}t}.$$

Consequently the entire time evolution operator can be decomposed to a product of two-site operators by performing a single Suzuki-Trotter decomposition

$$e^{-i\hat{H}t} = e^{-i\hat{H}_{\text{odd}}t}e^{-i\hat{H}_{\text{even}}t} + \mathcal{O}(t^2) = \prod_{i=1}^{L-1} e^{-i\hat{O}^{[i,i+1]}t} + \mathcal{O}(t^2). \tag{21}$$

Notice that instead of using the Hamiltonian matrix of size $(d^L \times d^L)$, we use $L-1$ matrices of size $d \times d$ by exploiting the fact that the chain only has nearest neighbor interactions.

With the expression from equation (21) we can now evolve the spin chain trough (imaginary) time by consecutively applying two-site operators with time step Δt. A graphical representation of this process, known as *Time-Evolving Block Decimation* (TEBD) is shown in figure 7.

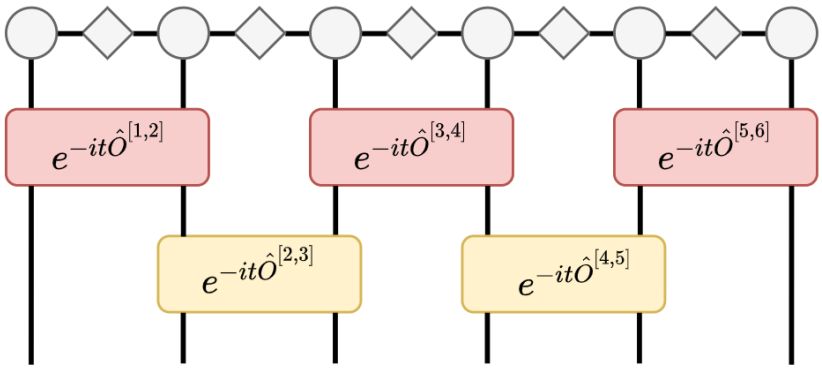

Figure 7: Application of a Hamiltonian on a spin chain of $L = 6$, red operators are part of $e^{-i\hat{H}_{odd}t}$, yellow operators are from $e^{-i\hat{H}_{even}t}$.

We have now finished the derivation of the TEBD algorithm and are able to evolve the MPS through time. However there is a last approximation we make to make it slightly easier for ourselves to compute the time evolution. Instead of working with matrix exponentials we will write the two-site operators in terms of matrices directly through the use of the Crank-Nicolson approximation, which states:

$$e^{-i\hat{O}\Delta t} = \left(\hat{\mathbb{I}} - \frac{i\hat{O}\Delta t}{2}\right)\left(\hat{\mathbb{I}} + \frac{i\hat{O}\Delta t}{2}\right)^{-1} + \mathcal{O}(\Delta t^3) \tag{22}$$

Recall that the error resulting from the Suzuki-Trotter approximation (equation 20) was of order $\mathcal{O}(\Delta t^2)$, thus the error over time evolution is governed by the Suzuki-Trotter approximation resulting in a global error of $\mathcal{O}(\Delta t)$ (aside from the error due to the truncation of the MPS).

4 Quantum Systems at Finite Temperature

Pure and Mixed States

A quantum system can be either in a *pure state* or a *mixed state*. Matrix Product States work with pure states, where the system can be fully described by a wavefunction $|\psi\rangle$ represented by a vector in the system's Hilbert space. In isolated systems the application of an operator maps the current state vector to another state vector in the same Hilbert space, this is not a problem. However, in real world situations a system is never isolated. There is always an environment present that interacts with the system, for example a heat bath or measurement device.

As previously stated an isolated system can always be described by a single vector $|\psi\rangle$ that follows a Hamiltonian $\hat{H}_S$. A non-isolated system, or open system, is a quantum system that is coupled to an external environment with Hamiltonian $\hat{H}_E$. This coupling is described by the coupling Hamiltonian $\hat{H}_{SE}$. Thus the system and environment are described by the total Hamiltonian $\hat{H} = \hat{H}_S + \hat{H}_E + \hat{H}_{SE}$. When the system is coupled to an environment it may become *entangled* with it, meaning that the system can no longer be described by a single wavefunction but is described by an ensemble of wavefunctions: a mixed state. Mixed states cannot be written as a vector but are instead defined by a *density matrix* $\hat{\rho} \equiv \sum_i p_i |\psi_i\rangle \langle\psi_i|$, where $|\psi_i\rangle$ are state vectors in the system Hilbert space and p_i are scalars subject to $\sum_i p_i = 1$.

4.1 Time Evolution and the Thermal Density Matrix

In isolated systems, the time evolution can be fully described by the TDSE (equation (5), repeated here for convenience), where the state at time t is related to the state at time 0 by

$$|\psi(t)\rangle = e^{-i\hat{H}t/\hbar} |\psi(0)\rangle \equiv \hat{U}(t) |\psi(0)\rangle .$$

Therefore the time evolution of the corresponding density matrix of this closed system is given as

$$\hat{\rho}(t) = |\psi(t)\rangle \langle\psi(t)| = e^{-i\hat{H}t/\hbar} |\psi(0)\rangle \langle\psi(0)| e^{i\hat{H}t/\hbar} = \hat{U}(t)\hat{\rho}(0)\hat{U}(t)^\dagger. \tag{23}$$

One might wonder why the time evolution of the density operator is relevant in the case of finite temperature spin chains. Before we tackle that, we must look at how a quantum system at finite temperatures is described. If $|\psi_i\rangle$ are the Hamiltonian eigenstates corresponding to eigenenergy E_i, then the probability for a system to be in state $|\psi_i\rangle$ is given by

$$p_i = \frac{e^{-\frac{E_i}{k_B T}}}{Z(\beta)} = \frac{e^{-\beta E_i}}{Z(\beta)},$$

where Z is the partition function

$$Z(\beta) = \sum_i e^{-\beta E_i} = \mathrm{Tr}(e^{-\beta \hat{H}}).$$

Combining these two formulas with the definition of the density matrix results in the following formula for the thermal density matrix $\hat{\rho}_\beta$:

$$\hat{\rho}_\beta = \sum_i p_i |\psi_i\rangle \langle\psi_i| = \sum_i \frac{e^{-\beta E_i}}{Z(\beta)} |\psi_i\rangle \langle\psi_i| = \frac{e^{-\beta \hat{H}}}{Z(\beta)}. \tag{24}$$

Let us now analyse the thermal density matrix at infinite temperature ($\beta = 0$). In this case the operator in the exponential becomes a matrix of only zeros: $e^{-\beta \hat{H}} = e^{\hat{0}} = \hat{\mathbb{I}}$. Substituting this result into equation (24) yields $\hat{\rho}_0 = \frac{\hat{\mathbb{I}}}{Z(0)}$, the maximally mixed state [11].

If we rewrite equation (24) in the following way:

$$\hat{\rho}_\beta = \frac{Z(0)}{Z(0)Z(\beta)} e^{\frac{-\beta \hat{H}}{2}} \hat{\mathbb{I}} e^{\frac{-\beta \hat{H}}{2}} = \frac{Z(0)}{Z(\beta)} e^{\frac{-\beta \hat{H}}{2}} \hat{\rho}_0 e^{\frac{-\beta \hat{H}}{2}} \tag{25}$$

and compare it to equation (23) we see that the finite temperature density matrix $\hat{\rho}_\beta$ can be found by evolving the density matrix at infinite temperature ρ_0 through imaginary time [14, 18]. This observation is crucial as it

forms the basis of our analysis. Explicitly, disregarding the factor $\frac{Z(0)}{Z(\beta)}$ in front, by evolving the system through imaginary time to $t = -i\hbar\beta/2$, equation (23) becomes equation (25). Thus we have found a way to describe quantum systems at finite temperatures. Real time evolution of the system is then calculated as expected[19]:

$$\hat{\rho}_\beta(t) = \hat{U}(t)\hat{\rho}_\beta(0)\hat{U}^\dagger(t). \tag{26}$$

It is important to keep in mind that by calculating time evolution this way we make an implicit assumption: we assume that the temperature remains constant over time: the time evolution of the system is *adiabatic*.

4.2 Analytical Solution using the Thermal Density Matrix

In equation (24) we found that the thermal density matrix is defined as $\hat{\rho}_\beta = \frac{e^{-\beta\hat{H}}}{Z(\beta)}$. To evaluate this expression we must find the exponential of a matrix. The matrix exponential is defined similar to the normal exponential function: if A is a square matrix and $t \in \mathbb{C}$, then [20]

$$e^{At} = \sum_{n=0}^{\infty} \frac{A^k t^k}{k!}. \tag{27}$$

In nontrivial cases calculating this series exactly might prove difficult. Luckily however, if our matrix A is *diagonizable* there is another method for calculating (27).

Theorem 1 *Let A a diagonizable matrix such that $A = PDP^{-1}$, where P is the column matrix containing the eigenvectors of A and D a diagonal matrix containing the corresponding eigenvalues*

$$P = \begin{bmatrix} \uparrow & \uparrow & & \uparrow \\ \underline{v}_1 & \underline{v}_2 & \dots & \underline{v}_n \\ \downarrow & \downarrow & & \downarrow \end{bmatrix} \qquad D = \begin{bmatrix} \lambda_1 & & & \\ & \lambda_2 & & \\ & & \ddots & \\ & & & \lambda_n \end{bmatrix}.$$

Then $\forall t \in \mathbb{C}$:

$$e^{At} = Pe^{Dt}P^{-1}, \tag{28}$$

where

$$e^{Dt} = \begin{bmatrix} e^{\lambda_1 t} & & & \\ & e^{\lambda_2 t} & & \\ & & \ddots & \\ & & & e^{\lambda_n t} \end{bmatrix}.$$

Proof: The proof can be found in [20].

This theorem allows us to easily calculate the thermal density matrix at any temperature provided we are able to diagonalize the Hamiltonian. The catch is that direct diagonalization of the Hamiltonian is only feasible for very small chains. More efficient methods that make use of the sparsity of the Hamiltonian allow us to stretch this for slightly longer chains, however the need for algorithms such as MPS eventually becomes unavoidable, see [21].

Even so, provided that we are able to diagonalize the Hamiltonian, we can easily calculate the thermal density matrix and the time evolution of the thermal density matrix defined in equation (26), which is repeated here for convenience

$$\hat{\rho}_\beta(t) = \hat{U}(t)\hat{\rho}_\beta(0)\hat{U}^\dagger(t).$$

Where $\hat{U}(t) = e^{-i\hat{H}t}$ can also be calculated using the found diagonalization of $\hat{H}$. Lastly, the expectation value of an operator $\hat{O}$ is calculated form the density matrix $\hat{\rho}$ by

$$\langle\hat{O}\rangle = \mathrm{Tr}(\hat{\rho}\,\hat{O}).$$

4.3 State Purification

It is our aim to describe density matrices using MPS, however MPS in its standard form works for state vectors. It is possible to extend the notion of matrix product states to operators[4, 22] and work with these directly or to describe finite temperature states probabilistically with a specific selection of pure quantum states[23], however one of the most effective ways is to describe a density operator of a mixed state as a single pure state, which can be done by a process called *purification*[11]. In simple terms, purification means that instead of describing a mixed state in the system Hilbert space with a density matrix, we describe it as a pure state defined on a different, larger Hilbert space. For illustration, consider a system S with Hilbert space $\mathcal{H}_S$ that is entangled with an environment E with Hilbert space $\mathcal{H}_E$. We then define the universe U as the system and environment together: $\mathcal{H}_U = \mathcal{H}_S \otimes \mathcal{H}_E$. A mixed state $\hat{\rho}_S$ existing solely in S can be obtained from a suitably constructed a *pure state* $|\psi_U\rangle \in \mathcal{H}_U$, where $|\psi_U\rangle$ is chosen in such a way that $\hat{\rho}_S = \mathrm{Tr}_E(|\psi_U\rangle \langle\psi_U|)$.

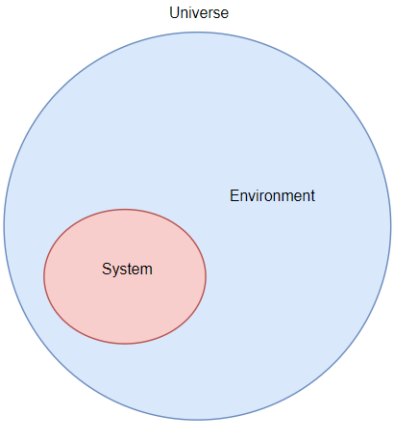

Figure 8: Visual representation of a system, environment and universe. Observe that if the system is in a mixed state with the environment, the universe is still in a pure state.

It seems that we require a complete description of the environment to implement this. However purification can also be done by making use of an *ancillary system* A. This is a fictitious system that represents the thermal bath, the sole purpose of which is enable us to find a pure state which is is compatible with our given mixed state in S, done by introducing new degrees of freedom. To purify the system S we can take the ancillary system A to be an exact copy of S. Suppose we have an orthonormal basis for S which we denote as $\{|i_S\rangle\}$. We take the same basis for the ancillary system: $\{|i_A\rangle\}$. If we now have a state in S that is described by $\hat{\rho}_S = \sum_i p_i |i_S\rangle \langle i_S|$ we define the purified state

$$|\psi\rangle = \sum_i \sqrt{p_i} |i_S\rangle |i_A\rangle . \tag{29}$$

To obtain our original density matrix ρ_S we construct the density matrix of the purified state and take the trace over the ancillary degrees of freedom.

As is shown in equation (25), finding the system's density matrix at a finite temperature can be done by evolving the infinite-temperature maximally mixed state $\hat{\rho}_0$ through imaginary time by applying the operator $\hat{U}(\beta) \equiv e^{\frac{-\beta \hat{H}}{2}}$. However, we can also apply this operator to the purification $|\psi\rangle$ from equation (29). Assume we have a purification $|\psi_0\rangle$ of $\hat{\rho}_0$ then we can find the purified state $|\psi_\beta\rangle$ at a finite temperature:

$$|\psi_\beta\rangle = e^{\frac{-\beta \hat{H}}{2}} |\psi_0\rangle . \tag{30}$$

This procedure leaves the question what the Hamiltonian of the combined physical-auxiliary system should be. Since our ancillary system A is purely theoretical we may choose *any site-local unitary operator* to act on A[24], since the physical system depends on the trace over A and is therefore not affected by the ancillary Hamiltonian, as long as it is unitary[25]. An obvious first choice would be to use the unit operator:

$$\hat{H} = \hat{H}_S \otimes \hat{\mathbb{I}}. \tag{31}$$

However, for dynamical models (where the system is evolved through real time at a finite temperature) this choice leads to rapid entanglement growth, limiting the timescale of the simulation[25]. A solution to this is presented in[24], where the Hamiltonian is chosen to be

$$\hat{H} = \hat{H}_S \otimes \hat{\mathbb{I}} - \hat{\mathbb{I}} \otimes \hat{H}_S, \tag{32}$$

thus as the system evolves forward in time the ancilla's evolve backward. More complicated methods exist involving operators that actively disentangle the system, see for example [26].

State Purification and Matrix Product States

Suppose we have a spin chain with L sites that can each be in d possible states, where each site has a local orthonormal basis $\{|n_i\rangle\}$. Then a general pure state can be written as in equation (11):

$$|\psi\rangle = \sum_{n_1 n_2 ... n_L} A^{[1]}_{n_1} A^{[2]}_{n_2} ... A^{[L]}_{n_L} |n_1 n_2 ... n_L\rangle .$$

Matrix product states were designed for pure states. Thus if the chain is in a mixed state it must first be purified. We do this by creating an exact copy of the chain in ancillary space and linking each site of the physical chain to its corresponding site of the ancillary chain. To obtain a description for the system at a finite temperature we start with the maximally mixed state at infinite temperature and evolve through imaginary time to the desired temperature as described in the previous section. Thus we must find a description of our purified system at $\beta = 0$.

At infinite temperature we found the system density matrix to be $\hat{\rho}_0 = \frac{1}{d^L}\hat{\mathbb{I}} = (\frac{1}{d}\hat{\mathbb{I}}_{2\times 2})^{\otimes L}$. This density matrix can be factorized, and therefore the system can be purified by locally purifying each physical site in the chain [14]. If we denote $|\psi_{i0}\rangle$ as the purification of $\hat{\rho}_0$ at site i, then we can write the wavefunction of the purified chain as a product state $|\psi_0\rangle = |\psi_{10}\rangle ... |\psi_{L0}\rangle$.

Let us now consider a single site i, where the physical state is denoted by $|n_i\rangle$ and the ancillary state by $|n'_i\rangle$. The physical and ancillary site together form a pure state $|\psi_{i0}\rangle$ which is derived from the density matrix by using that $\hat{\rho}_{i0} = \mathrm{Tr}_A(|\psi_{i0}\rangle \langle\psi_{i0}|)$:

$$\frac{1}{d}\hat{\mathbb{I}} = \sum_{n_i} \frac{1}{d} |n_i\rangle \langle n_i| = Tr_A\Big[\Big(\sum_{n_i,n'_i} \frac{1}{\sqrt{d}} |n_i\rangle |n'_i\rangle \delta_{n_i,n'_i}\Big)\Big(\sum_{n_i,n'_i} \frac{1}{\sqrt{d}} \langle n_i| \langle n'_i| \delta_{n_i,n'_i}\Big)\Big],$$

thus

$$|\psi_{i0}\rangle = \sum_{n_i,n'_i} \frac{1}{\sqrt{d}} |n_i\rangle |n'_i\rangle \delta_{n_i,n'_i}. \tag{33}$$

Since we work with spin-$\frac{1}{2}$ particles this is equivalent to the following linear combination of triplet states:

$$|\psi_{i0}\rangle = \frac{1}{\sqrt{2}} |\uparrow\uparrow\rangle + \frac{1}{\sqrt{2}} |\downarrow\downarrow\rangle ,$$

which is a *Bell state*. The initial state $|\psi_0\rangle = \bigotimes_{i=1}^{L} |\psi_{i0}\rangle$ of our purified spin-$\frac{1}{2}$ chain can be written in MPS form exactly with matrices of size (1×1). Specifically: $\Gamma^{[i]}_1 = \Gamma^{[i]}_4 = \Big[\frac{1}{\sqrt{2}}\Big]$, $\Gamma^{[i]}_2 = \Gamma^{[i]}_3 = \big[0\big]$ and $\Lambda^{[i]} = \big[1\big]$ $\forall i$. (Imaginary) time evolution will cause the size of the matrices to increase and eventually the need for truncation will arise. The truncation parameter χ is then a crucial parameter, as it must be balanced to maintain both accuracy and model efficiency.

5 Simulation Results

In the previous chapters the theory of studying spin chains at finite temperature has been discussed. Using the results from the theory a model has been made using python that is capable of simulating such systems. The python model is an extension build upon the already existing model created by A. Meló, P. Vree and J. Bouwmeester [5, 15, 16]. The simulation is characterized by a small number of parameters: the chain length L, the truncation parameter χ, the magnetic field strength h, the temperature T and the Hamiltonian of the auxiliary system. The focus of this section is studying the effect of these parameters on various physical quantities and discussing our findings. The simulations are performed for small chains and are compared to the analytical solution.

5.1 Imaginary Time Evolution

We will begin by examining what happens to the system as it evolves through imaginary time. That is to say, as it evolves from the infinite temperature mixed state to the desired finite temperature state. In figure 9 the expected energy of the system is shown as a function of the temperature, as well as the error of the simulation.

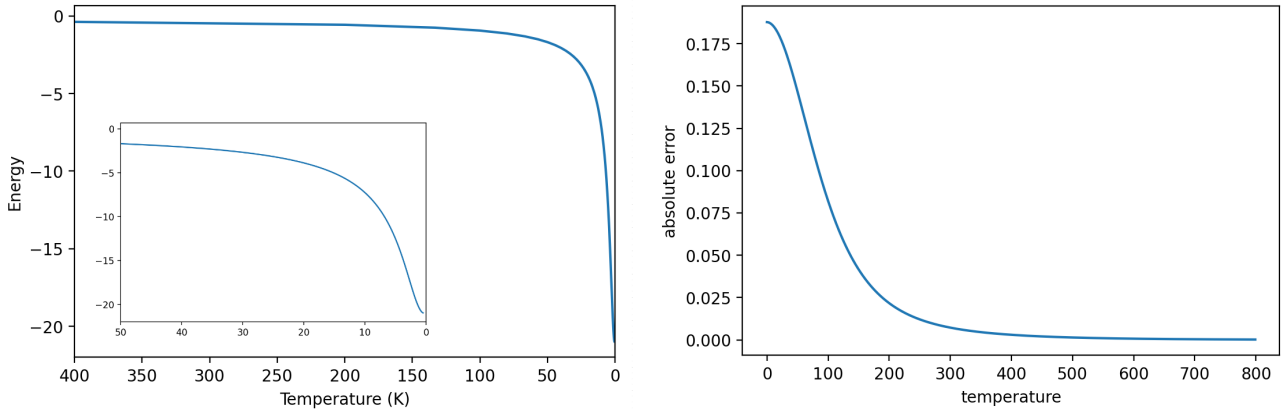

(a) Expected energy of the chain during MPS simulation.

(b) Error of the MPS simulation, $\Delta\beta = 0.00125$.

Figure 9: Expected energy of the chain compared to system temperature and the error compared to the exact solution at each time step.
$L = 7$, $\chi = 24$, $h = 3$.

We immediately see from 9b that the error of the MPS simulation compared to the exact solution tends to 0 as the temperature decreases. Relatively the error is even higher at high temperatures as the energy is closer to 0 but also decreases along with the temperature. At $T = 0.5$, the lowest temperature reached during the simulation, the relative error is of order 10^{-6}.

From figure 9a we observe that for higher temperatures the energy of the system rapidly increases and tends towards zero for infinite temperatures. Because of the Hamiltonian chosen (equation (6)) the energy of the system is closely related to the spin of the system. In figure 10 the average of $\langle \hat{S}_z \rangle$ (the magnetization) over the entire chain is shown over the same timescale.

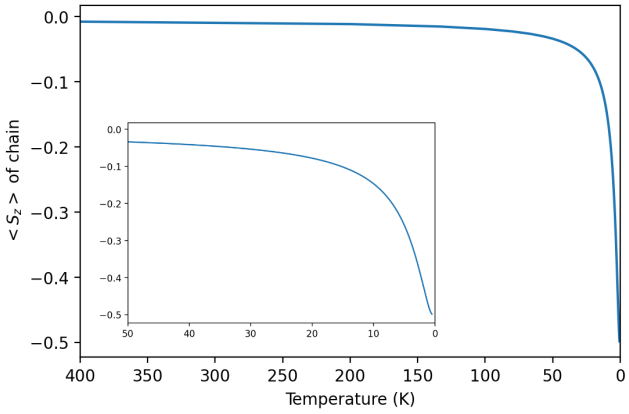

(a) $\langle \hat{S}_z \rangle$ of the chain during MPS simulation.

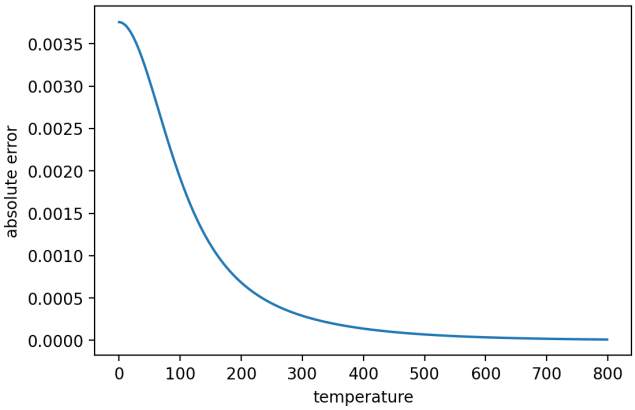

(b) Error of the MPS simulation, $\Delta\beta = 0.00125$.

Figure 10: $\langle S_z \rangle$ averaged over the entire chain compared to the system temperature and the error compared to the exact solution at each time step.
$L = 7$, $\chi = 24$, $h = 3$

We see that, apart from a scaling difference figures 9 and 10 are nearly identical. Meanwhile $\langle \hat{S}_x \rangle$ and $\langle \hat{S}_y \rangle$ remain at 0, with deviations of order of magnitude 10^{-15} for these simulations.

From these facts we can conclude that the energy of the system for different temperatures is governed almost entirely by $\langle \hat{S}_z \rangle$. However the magnetization of the chain is governed by the strength of the magnetic field h. In figure 11 the effect of the magnetic field on the spins is shown for different temperatures.

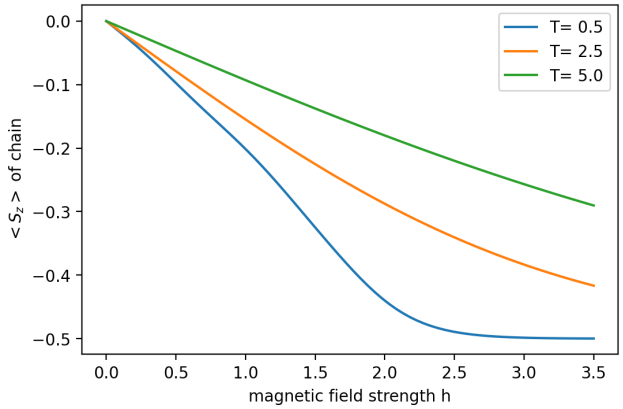

(a) $\langle \hat{S}_z \rangle$ of the chain during MPS simulation.

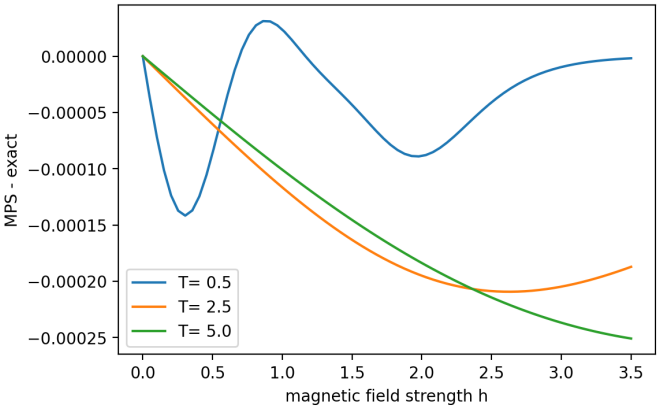

(b) Error of the MPS simulation.

Figure 11: $\langle S_z \rangle$ averaged over the entire chain as a function of the magnetic field at varying temperatures and the error compared to the exact simulation.
$L = 6$, $\chi = 24$

We observe that at higher temperatures a stronger magnetic field is required in order to magnetize the chain. Thus the simulation result is in line with what we would physically expect.

In figure 11 the lowest temperature reached is $T = 0.5$ Kelvin. If we lower the temperature even further we obtain an interesting result, see figure 12a. When the temperature is sufficiently low the discrete nature of the spectrum is revealed. We see 3 distinct steps of equal height in the average expected $\hat{S}_z$ value of the chain. It can be verified this is related to chain size by performing the exact same simulation for a chain of $L = 10$, see figure 12b, which makes the spectrum more dense. We are easily able to discern 4 discrete levels. However, the last step is twice as long as the others and upon very close inspection it can be seen that the 'step' is not entirely straight either. In fact, it are two distinct steps, however the plateau in between is so small that they can hardly be distinguished. The distinction between the fourth and fifth step can be revealed by lowering the temperature even further, see figure 12c. For a chain of $L = 6$ we see 3 distinct steps, for $L = 10$ we see 5, so we may safely assume the chain length is the cause of this behaviour. We also observe that the plateau between steps becomes smaller for higher h. In other words: the magnetization of the chain increases more rapidly the stronger the

magnetic field becomes, until the chain is fully magnetized and the magnetization remains constant. In figure 12d this can be seen more clearly. Here the length of the chain is such that the discrete levels can no longer be distinguished at this temperature.

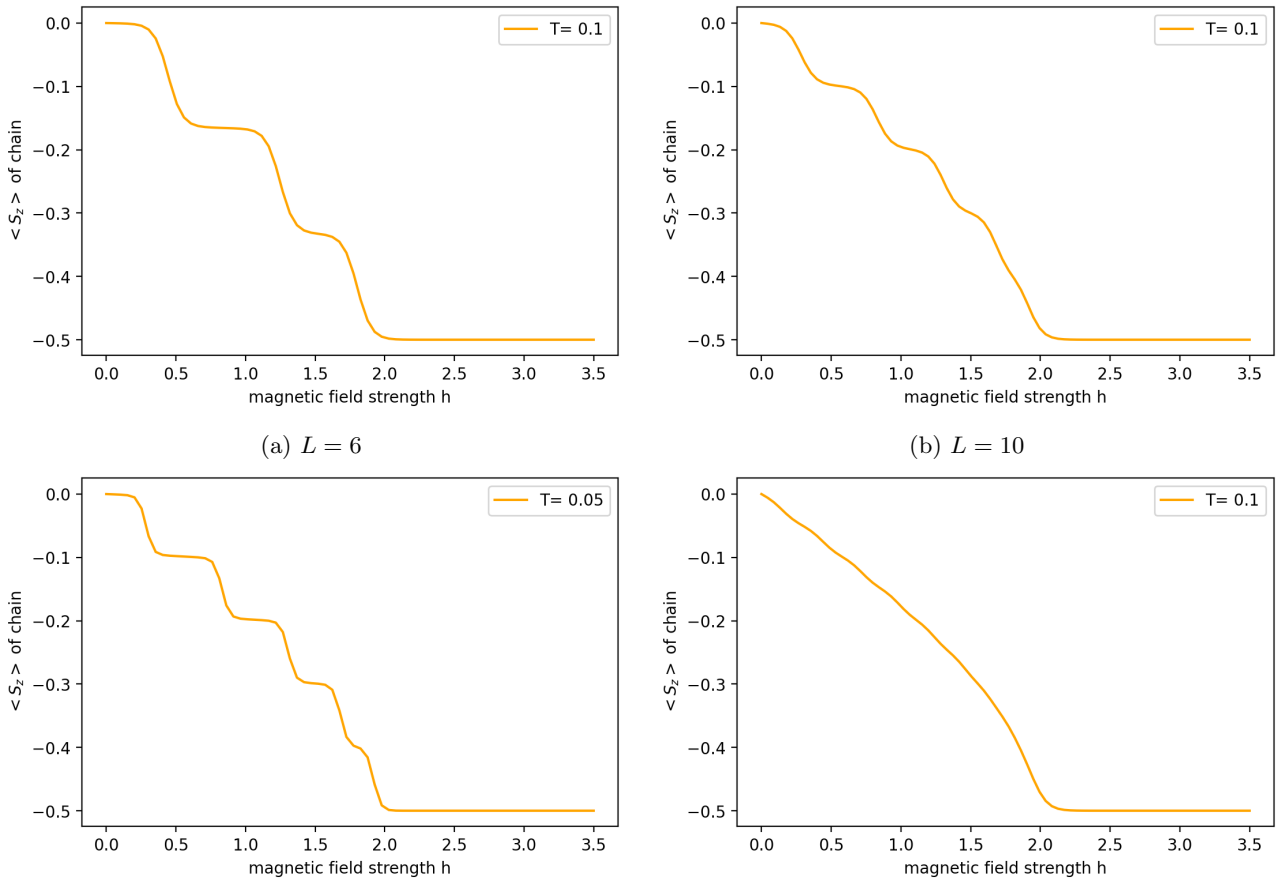

(a) $L = 6$ (b) $L = 10$

(c) $L = 10$ (d) $L = 20$

Figure 12: At low temperatures the discreteness of the spin chain is revealed.
$\chi = 12$

Interestingly, simulating a spin chain without the use of an ancillary system yields comparable results. In this case we also cannot start the simulation with a maximally mixed state. Instead we generate a random state with $s = \frac{1}{2}$ and apply imaginary time evolution to it with the same time steps as used for the previously obtained results in figures 11 and 12, the results are displayed in figure 13. Due to the the randomized initial state of the system the outcome of the simulations is inconsistent, thus three separate simulations are shown.

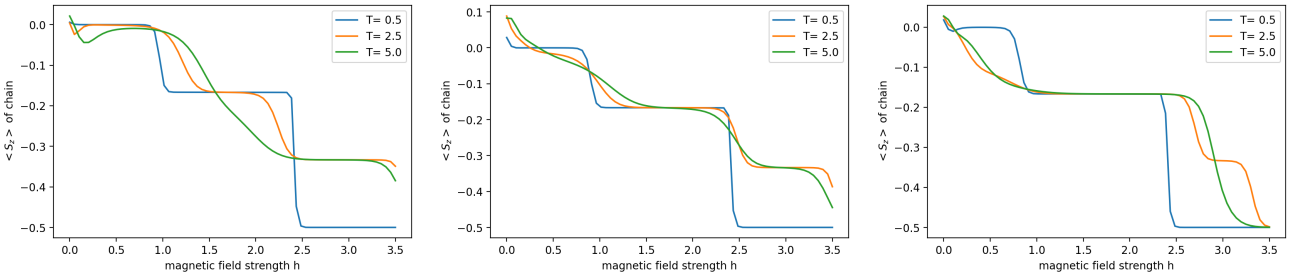

(a) (b) (c)

Figure 13: Simulations of a spin chain without the use of purification.
$L = 6$, $\chi = 20$

By far the most consistent is the case $T = 0.5$, where the chain magnetization goes down in three steps at roughly the same magnetic field strength each time. The other two exhibit less reproducible behaviour.

The magnetization also decreases step-wise but the drops are of varying height and occur at varying locations. Moreover, sometimes the system is more magnetized at higher temperatures than at lower temperatures with the same magnetic field strength. For example in 13a the order is flipped right before $h = 2.5$. The differences with simulations using purification (figure 11) can clearly be seen.

5.2 Real Time Evolution

When evolving the exact solution through real time the expected values for the energy, total spin and spin in all 3 three directions *remain constant*. With this knowledge in mind, let us examine the time evolution of the MPS.

We start again by considering the total energy and the spin $\langle \hat{S}_z \rangle$ of the MPS simulation in figure 14. All simulations in this section are obtained with a time step of 0.01 seconds.

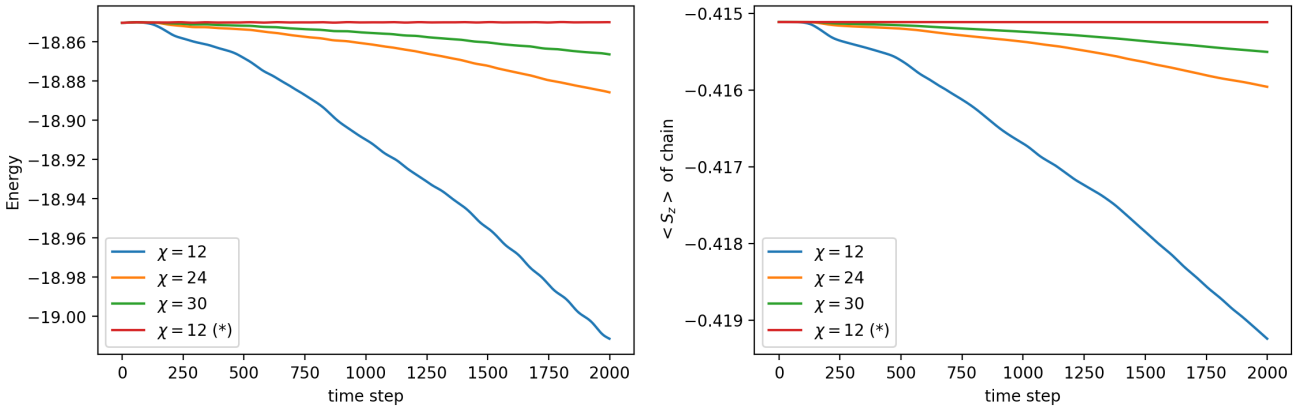

(a) Expected energy of the chain over time

(b) Average $\langle \hat{S}_z \rangle$ of the chain over time

Figure 14: Time evolution of a chain of length 7. The blue, orange and green lines are simulations where the system Hamiltonian is given by equation (31) (the ancilla's Hamiltonian is the identity), the red line (*) is a simulation where the system Hamiltonian is that of equation (32) (the ancilla's evolve backwards in time). $L = 7$, $h = 3$, $T = 2$

In these figures the effect of evolving the auxiliary system backwards through time is clearly shown. The blue, orange and green lines are from a simulation using a Hamiltonian as in equation (31) and the red line with a Hamiltonian as in (32). The normalization of the state over time also follows this pattern, see figure B.2.

We observe that simulations with larger χ values (in the case of $\hat{H}_A = \hat{\mathbb{I}}$) stay constant for longer and decrease more gradually, at the expense of longer computation time. In other words they appear to converge to a constant value. This is as expected since the exact solution remains constant over time. In [24] it is mentioned that evolving the ancillary system backwards through time counteracts the growth in entanglement, see equation (32). Highly entangled states require more numerical resources to be accurately described by an MPS (since they are volume law states). Thus we obtain more stable results by increasing χ or by limiting the entanglement growth.

However the effect of using reverse time evolution for the ancilla's can be more clearly seen if we study the time evolution of $\langle \hat{S}_z \rangle$ for each site in the chain independently, see figure 15. If the ancilla's do not evolve with time (figures 15a and 15b) we see the influence of a higher truncation parameter χ very clearly: in the case $\chi = 12$ oscillations start becoming rather chaotic very swiftly, but for $\chi = 24$ this is less obvious. In the case where the ancilla's evolve through reverse time (figures 15c and 15d) there is little difference between $\chi = 12$ and $\chi = 24$, indicating that $\chi = 12$ is a sufficiently large truncation parameter for this chain and timescale. In fact, in figure B.1 we see that even $\chi = 6$ provides comparable results up to time step 500. Note that in all simulations during the first few time steps (up to about step 100) the results are the same. After this point the model the results of the first two simulations begin to deviate due to the more rapid entanglement growth between sites over time. A simulation over a longer time span can be found in the appendix: see figure B.3.

It is important to keep in mind that according to the analytical solution $\langle \hat{S}_z \rangle$ should remain constant over time. There is little difference between figures 15c and 15d thus the oscillations are a result the Suzuki-Trotter or Crank-Nicolson approximations, which is dependent on the size of the time step. In figure B.4 we observe that a lower time step indeed decreases the amplitude of the oscillations.

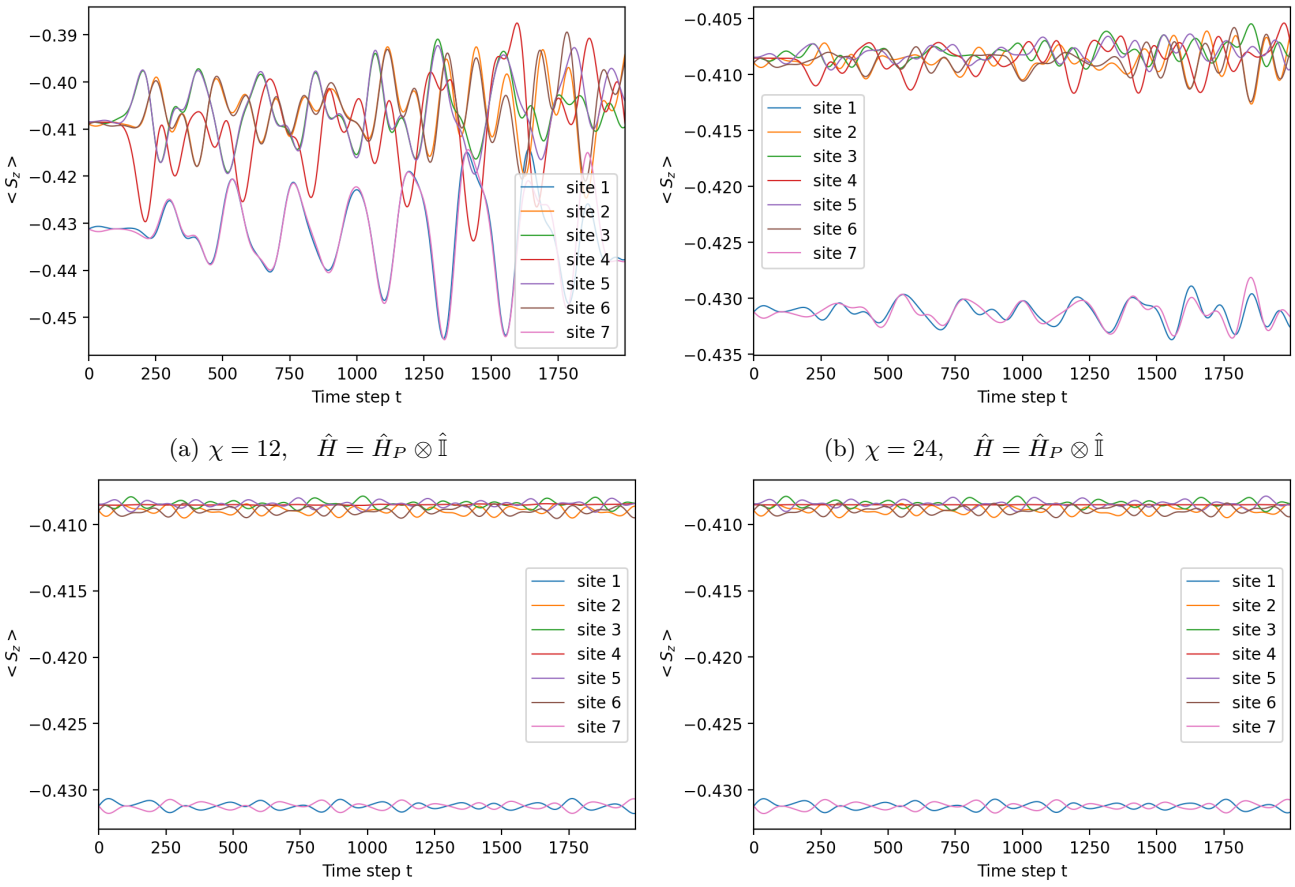

(a) $\chi = 12, \quad \hat{H} = \hat{H}_P \otimes \hat{\mathbb{I}}$

(b) $\chi = 24, \quad \hat{H} = \hat{H}_P \otimes \hat{\mathbb{I}}$

(c) $\chi = 12, \quad \hat{H} = \hat{H}_P \otimes \hat{\mathbb{I}} - \hat{\mathbb{I}} \otimes \hat{H}_P$

(d) $\chi = 24, \quad \hat{H} = \hat{H}_P \otimes \hat{\mathbb{I}} - \hat{\mathbb{I}} \otimes \hat{H}_P$

Figure 15: Time evolution of $\langle \hat{S}_z \rangle$ of each site in the chain for the two different Hamiltonians. $L = 7$, $h = 3$, $T = 2$

Influence of the system parameters

Upon closer inspection of the lower two figures we see that there are pairs of sites that have identical oscillations in opposite directions. These pairs are sites 1 and 7, 2 and 6, and 3 and 5. Site 4, which is exactly in the middle, remains (almost) constant (and thus closest to the exact simulation). These plots are slightly cluttered, thus the same results are shown for only the middle three sites of the chain in figure 17a.

Furthermore, we observe that the expected value for $\hat{S}_z$ is slightly lower for the sites at the edge than for the sites in the middle. A logical explanation is the fact that the sites at the ends of the chain are coupled to only one other site instead of two, thus the magnetic field has a comparatively greater influence on these sites compared to sites not at the boundaries.

To highlight the influence of the temperature on the simulation results we execute the same simulation as in 15a, but for $T = 0.5$. At lower temperatures the system is less entangled with the environment and thus the ancilla's (and their time evolution) have less influence. We observe that in this case the system can be simulated adequately without the backward time propagation of the ancillas, see figure 16.

Another observation we make here is that the expected values for $\hat{S}_z$ are shifted compared to figure 15. It can now be clearly seen that spins located towards the ends of the chain are more magnetized than those closer to the chain center.

Up to now we have studied the effects of different Hamiltonians, truncation parameters and temperatures on the simulation. Let us now see what happens if we increase the length of the chain (with Hamiltonian $\hat{H} = \hat{H}_P \otimes \hat{\mathbb{I}} - \hat{\mathbb{I}} \otimes \hat{H}_P$). The results are shown in figure 17. We observe that the middle site fluctuates more strongly. Running the simulation with a higher χ smoothens these fluctuations as shown in figure B.5. Thus

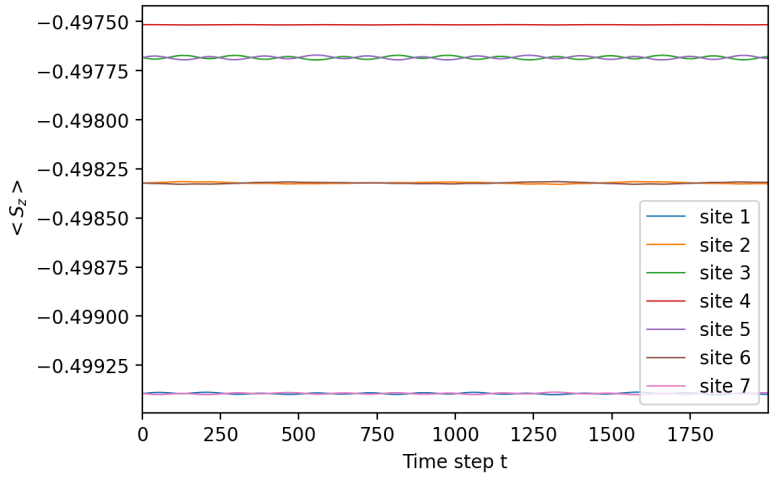

Figure 16: Time evolution of $\langle \hat{S}_z \rangle$ for each site in the chain with Hamiltonian $\hat{H} = \hat{H}_P \otimes \hat{\mathbb{I}}$.
$L = 7$, $\chi = 12$, $T = 0.5$

even when using reverse time propagation for the auxiliary system the system size is a limiting factor, requiring more computational resources for accurate results.

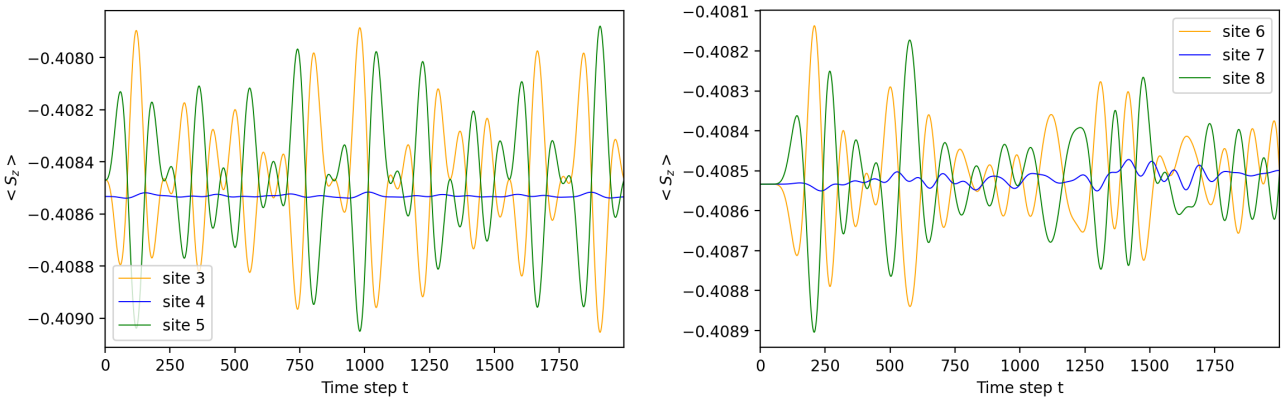

(a) $L = 7$ (b) $L = 13$

Figure 17: Expected values of $\langle \hat{S}_z \rangle$ of the middle three sites in the chain for two different chain lengths.
$\chi = 24$, $h = 3$, $T = 2$

A detail we should pay attention to are the results for the system at high temperatures. Since $\beta = \frac{1}{T}$ a high temperature means a very low β and therefore the imaginary time evolution is only over a very short time span. Simulating a chain with $L = 7$ for $T = 20$ yields almost the exact same results as for $T = 20000$, apart from a shift of the time average and a scaling of the amplitudes, see figure B.6.

We have also noticed in chains of odd length that the $\langle \hat{S}_z \rangle$ of the sites 'oscillate' pairwise in opposite directions. For even chains similar behaviour occurs. In this case the $\langle \hat{S}_z \rangle$ of the pairs (again constituted of spins at equal distance from the center of the chain) are exactly the same, see figure 18.

On a last note the time evolution of $\langle \hat{S}_x \rangle$ and $\langle \hat{S}_y \rangle$ must be mentioned. Over time both remain constant around 0 within numerical accuracy, however, with some exponential increase for longer times, as can be seen in the log-scale plots of figure B.7. It is not surprising that these remain around 0 due to the fact that the system is isotropic for rotations around the z-axis.

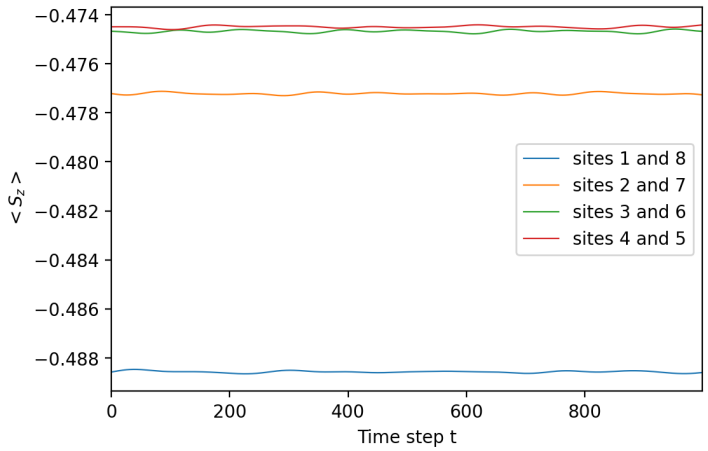

Figure 18: Expected values of $\langle \hat{S}_z \rangle$ for a chain of even length. $\chi = 24$, $h = 3$, $T = 1$

6 Summary and Conclusions

The aim of this work was to simulate spin chains at finite temperatures. We formulated our spin chain using matrix product states and were therefore able to efficiently approximate our state and make use of the powerful TEBD algorithm. We then combined this with the concept of purification in order to describe (incoherent) thermal states as pure states, defined using an auxiliary system. The combination of MPS, purification and TEBD allowed us to simulate spin chains at finite temperatures.

We used an XY-Hamiltonian with a magnetic field in the z-direction to test our model. The influence of nonzero temperatures on chain magnetization due to the magnetic field was clearly demonstrated. Moreover, we have seen the effect that reverse time evolution of the auxiliary system has on the reachable timescale during real-time simulations, even when using modest computational resources. The results of the simulations using MPS, have been verified at small scales by comparing them to the analytical solution of the problem, which was calculated directly using the density matrix.

During the imaginary time evolution the MPS simulations proved to be very accurate, especially for lower temperatures. During real time evolution the model deviated from the exact solution. Although the energy and the total $\langle \hat{S}_z \rangle$ of the chain remained constant, the local expectations for $\langle \hat{S}_z \rangle$ started oscillating. This oscillation is a consequence of both the truncation and the error due to the Suzuki-Trotter (and to a lesser extent the Crank-Nicolson) approximation, of order $\mathcal{O}(\Delta t)$ globally. Even so, due to the origin of the error, the model can be made more precise by simply increasing the truncation parameter χ and decreasing the (real) time step. Naturally, this comes at the cost of a longer model running time. However, the major gain of using matrix product states over the analytical solution is during the simulation of larger systems, in which case the diagonalization of the Hamiltonian becomes excessively difficult to compute. Even for a chain of $L = 13$ the MPS simulation with $\chi = 24$ is faster than the direct computation (for $L = 13$ the Hamiltonian is a matrix of dimensions (8192×8192)).

In this research we have worked under the assumption that the system remains in thermal equilibrium during real time evolution. Thus, a possible extension for this model could be the incorporation of thermal noise. Especially at low temperatures we found this to be important, which is to be expected since small temperature fluctuations can be of great impact to β. Other possible subjects of further research might include the modeling of temperature differences throughout a chain, or to attempt to replicate experimental data in a specific situation.

References

[1] S. R. White, "Density matrix formulation for quantum renormalization groups," *Phys. Rev. Lett.*, vol. 69, pp. 2863–2866, Nov 1992.

[2] G. Vidal, "Efficient simulation of one-dimensional quantum many-body systems," *Phys. Rev. Lett.*, vol. 93, jul 2004.

[3] F. Verstraete, D. Porras, and J. I. Cirac, "Density matrix renormalization group and periodic boundary conditions: A quantum information perspective," *Phys. Rev. Lett.*, vol. 93, nov 2004.

[4] F. Verstraete, J. J. García-Ripoll, and J. I. Cirac, "Matrix product density operators: Simulation of finite-temperature and dissipative systems," *Phys. Rev. Lett.*, vol. 93, nov 2004.

[5] J. Bouwmeester, *Time Evolution of a Device for Remote Detection on Atomic Spin Chains using Matrix Product States*. Bachelor's thesis, Jul 2020.

[6] R. Elbertse, D. Coffey, J. Gobeil, and A. Otte, "Remote detection and recording of atomic-scale spin dynamics," *Commun. Phys.*, vol. 3, p. 94, 05 2020.

[7] M. Białończyk, F. Gómez-Ruiz, and A. del Campo, "Exact thermal properties of free-fermionic spin chains," *SciPost Physics*, vol. 11, jul 2021.

[8] E. Lieb, T. Schultz, and D. Mattis, "Two soluble models of an antiferromagnetic chain," *Ann. Phys.*, vol. 6, no. 3, pp. 407–466, 1961.

[9] A. Blum, J. E. Hopcroft, and R. Kannan, *Foundations of Data Science*. Cambridge University Press, 2020.

[10] F. Pollmann, "Efficient numerical simulations using matrix-product states," 2016. http://quantumtensor.pks.mpg.de/wp-content/uploads/2016/06/notes_1.pdf.

[11] M. A. Nielsen and I. L. Chuang, *Quantum Computation and Quantum Information*. Cambridge University Press, 2000.

[12] J. A. Bengua, *Matrix product state decomposition in machine learning and signal processing*. PhD thesis, 2016. https://opus.lib.uts.edu.au/bitstream/10453/120359/2/02whole.pdf.

[13] M. B. Hastings, "An area law for one-dimensional quantum systems," *J. Stat. Mech.*, vol. 2007, pp. P08024–P08024, aug 2007.

[14] U. Schollwöck, "The density-matrix renormalization group in the age of matrix product states," *Ann. Phys.*, vol. 326, pp. 96–192, jan 2011.

[15] A. Melo, *Numerical study of a superconducting qubit for the realization of quantum Ising chains using matrix product state techniques*. Master's thesis, Sep 2017.

[16] P. Vree, *Computing the Ground-State Energy of the Ising Model in a Transverse Field with Matrix Product States*. Bachelor's thesis, Jul 2018.

[17] M. Suzuki, "Generalized Trotter's formula and systematic approximants of exponential operators and inner derivations with applications to many-body problems," *Comm. Math. Phys.*, vol. 51, no. 2, pp. 183 – 190, 1976.

[18] S. Paeckel, T. Köhler, A. Swoboda, S. R. Manmana, U. Schollwöck, and C. Hubig, "Time-evolution methods for matrix-product states," *Ann. Phys.*, vol. 411, p. 167998, dec 2019.

[19] T. Barthel, U. Schollwöck, and S. Sachdev, "Scaling of the thermal spectral function for quantum critical bosons in one dimension," 2012.

[20] D. Surowski and A. Mohammad, "Lecture notes advanced linear algebra," jul 1997. https://www.math.ksu.edu/ dbski/writings/Linear_Algebra.pdf.

[21] R. Slooter, *Diagonalizing Quantum Spin Chains*. Bachelor's thesis, Jul 2015.

[22] I. P. McCulloch, "From density-matrix renormalization group to matrix product states," *J. Stat. Mech.*, vol. 2007, pp. 10014–10014, oct 2007.

[23] E. M. Stoudenmire and S. R. White, "Minimally entangled typical thermal state algorithms," *New J. Phys.*, vol. 12, p. 055026, may 2010.

[24] C. Karrasch, J. H. Bardarson, and J. E. Moore, "Finite-temperature dynamical density matrix renormalization group and the drude weight of spin-1/2 chains," *Phys. Rev. Lett.*, vol. 108, may 2012.

[25] C. Karrasch, J. H. Bardarson, and J. E. Moore, "Reducing the numerical effort of finite-temperature density matrix renormalization group calculations," *New J. Phys.*, vol. 15, p. 083031, aug 2013.

[26] J. Hauschild, E. Leviatan, J. H. Bardarson, E. Altman, M. P. Zaletel, and F. Pollmann, "Finding purifications with minimal entanglement," *Phys. Rev. B*, vol. 98, dec 2018.

A Maximizing Overlap Between Matrix Product States

In [4] a method is presented to maximize the overlap between two states written in MPS form with different bond dimensions. In this paper only a formula (equation (6)) is given without motivation. In this section the derivation of this formula is given, should it be required for further research.

Our aim is to truncate our matrices A_{n_i} while minimizing the loss of information due to this truncation. Moreover, aside from maximizing the overlap the normalization of the state must be maintained. In [4] a set of equations is presented without derivation that solves this exact problem

$$\sum_{\alpha',\beta'} C_{n_i}^{\alpha,\beta,\alpha',\beta'} \tilde{A}_{n_i}^{\alpha',\beta'} = H_{n_i}^{\alpha,\beta}. \tag{A.1}$$

We will derive this equation and present it in a slightly more shorthand notation.

Suppose the matrices A_{n_i} are of size $(D_i \times D_{i+1})$ and we define the truncated matrices as $\tilde{A}_{n_i}$ of size $(\tilde{D}_i \times \tilde{D}_{i+1})$ with $\tilde{D}_i \leq D_i \ \forall i$. Our original state is denoted as $|\psi\rangle$, the truncated state is $|\phi\rangle$

$$|\psi\rangle = \sum_{n_1 n_2 ... n_L} A_{n_1} A_{n_2} ... A_{n_L} |n_1 n_2 ... n_L\rangle \qquad |\phi\rangle = \sum_{n_1 n_2 ... n_L} \tilde{A}_{n_1} \tilde{A}_{n_2} ... \tilde{A}_{n_L} |n_1 n_2 ... n_L\rangle .$$

We can formulate the function we want to maximize as follows:

$$max_\phi \ \frac{|\langle\psi|\phi\rangle|^2}{\langle\psi|\psi\rangle \langle\phi|\phi\rangle}. \tag{A.2}$$

Since $|\psi\rangle$ is fixed and normalized $\langle\psi|\psi\rangle = 1$ and can be ignored. The norm $\langle\phi|\phi\rangle$ is present in the denominator in order to ensure the normalization of $|\phi\rangle$. The $|\phi\rangle$ that solves the optimization problem in (A.2) can be found by the standard procedure of taking the derivative with respect to each $\tilde{A}_{n_i}$ and setting it equal to zero. This is worked out below.

$$\frac{\partial}{\partial \tilde{A}} \frac{|\langle\psi|\phi\rangle|^2}{\langle\phi|\phi\rangle} = \frac{1}{\langle\phi|\phi\rangle} \frac{\partial |\langle\psi|\phi\rangle|^2}{\partial \tilde{A}} - \frac{|\langle\psi|\phi\rangle|^2}{(\langle\phi|\phi\rangle)^2} \frac{\partial \langle\phi|\phi\rangle}{\partial \tilde{A}} = 0$$

$$\langle\phi|\phi\rangle \frac{\partial |\langle\psi|\phi\rangle|^2}{\partial \tilde{A}} - \langle\phi|\psi\rangle \langle\psi|\phi\rangle \frac{\partial \langle\phi|\phi\rangle}{\partial \tilde{A}} = 0$$

We can rewrite the partial derivatives as follows:

$$\frac{\partial |\langle\psi|\phi\rangle|^2}{\partial \tilde{A}} = 2\mathrm{Re}\Big[\left\langle \psi \middle| \frac{\partial \phi}{\partial \tilde{A}} \right\rangle \langle\phi|\psi\rangle \Big] \qquad \frac{\partial \langle\phi|\phi\rangle}{\partial \tilde{A}} = 2\mathrm{Re}\Big[\left\langle \phi \middle| \frac{\partial \phi}{\partial \tilde{A}} \right\rangle \Big].$$

If we assume that the two elements in the Re[ ] expressions are real, the Re[ ] operator may be left out. Furthermore, after filling in these expressions the factor 2 may be divided away, resulting in

$$\langle\phi|\phi\rangle \langle\phi|\psi\rangle \left\langle \psi \middle| \frac{\partial \phi}{\partial \tilde{A}} \right\rangle - \langle\phi|\psi\rangle \langle\psi|\phi\rangle \left\langle \phi \middle| \frac{\partial \phi}{\partial \tilde{A}} \right\rangle = 0$$

or

$$\langle\psi|\phi\rangle \left\langle \phi \middle| \frac{\partial \phi}{\partial \tilde{A}} \right\rangle = \langle\phi|\phi\rangle \left\langle \psi \middle| \frac{\partial \phi}{\partial \tilde{A}} \right\rangle .$$

Suppose the truncated state $|\phi\rangle$ is initially chosen in such a way that it is already very close to $|\psi\rangle$, so $\langle\psi - \phi|\phi\rangle$ is very small (≈ 0). Let us make the assumption that this is the case, observe that we then have

$$\frac{\langle\psi|\phi\rangle}{\langle\phi|\phi\rangle} = \frac{\langle\psi - \phi|\phi\rangle + \langle\phi|\phi\rangle}{\langle\phi|\phi\rangle} = 1 + \frac{\langle\psi - \phi|\phi\rangle}{\langle\phi|\phi\rangle} \approx 1.$$

If we now divide out $\langle\phi|\phi\rangle$ from our previous equation we are left with

$$\left\langle \phi \middle| \frac{\partial \phi}{\partial \tilde{A}} \right\rangle = \left\langle \psi \middle| \frac{\partial \phi}{\partial \tilde{A}} \right\rangle . \tag{A.3}$$

The overlap between states $|\phi\rangle$ and $|\psi\rangle$ is calculated as follows[22]:

$$\langle\psi|\phi\rangle = Tr\Big(\sum_{\{n_i\}}(A^*_{n_1}\otimes\tilde{A}_{n_1})(A^*_{n_2}\otimes\tilde{A}_{n_2})\ ...\ (A^*_{n_L}\otimes\tilde{A}_{n_L})\Big). \tag{A.4}$$

In [4] they use the complex conjugate of this expression. Doing this is invariant to the result, thus we *will continue from this point the complex conjugate of expression* (A.4).

We are now going to rewrite equation (A.3) into a linear system of equations. First we define $E_i \equiv \sum_{n_i}\tilde{A}_{n_i}\otimes\tilde{A}^*_{n_i}$ and $G_i \equiv \sum_{n_i} A_{n_i}\otimes\tilde{A}^*_{n_i}$. Then we have

$$(\langle\psi|\phi\rangle)^* = Tr\Big(G_1...G_L\Big) \qquad\qquad (\langle\phi|\phi\rangle)^* = Tr\Big(E_1...E_L\Big).$$

We will evaluate the partial derivatives in equation (A.3) matrix by matrix and element by element. Recall that the matrix $\tilde{A}_{n_i}$ is of size $(\tilde{D}_i\times\tilde{D}_{i+1})$. Let us take the partial derivative to the i'th matrix in spin state n_i at the β'th element of the α'th row. We obtain the equation:

$$Tr\Big(E_1...E_{i-1}\ (\tilde{A}_{n_i}\otimes\Delta_{\alpha,\,\beta})\ E_{i+1}...E_L\Big) = Tr\Big(G_1...G_{i-1}\ (A_{n_i}\otimes\Delta_{\alpha,\,\beta})\ G_{i+1}...G_L\Big),$$

in which $\Delta_{\alpha\,\beta}$ is a matrix of zeros with a single 1 in row α and column β. We may use the fact that the trace is cyclic ($Tr(AB) = Tr(BA)$) to rewrite this as

$$Tr\Big((\tilde{A}_{n_i}\otimes\Delta_{\alpha,\,\beta})\ E_{i+1}...E_LE_1...E_{i-1}\Big) = Tr\Big((A_{n_i}\otimes\Delta_{\alpha,\,\beta})\ G_{i+1}...G_LG_1...G_{i-1}\Big).$$

There is now only one $\tilde{A}_{n_i}$ left in our expression. We will take this out by rewriting as a sum over each element in $\tilde{A}_{n_i}$ which, we will later see, will allow us to treat equation (A.3) as a system of linear equations. We obtain

$$\sum_{\alpha',\beta'} Tr\Big((\Delta_{\alpha',\,\beta'}\otimes\Delta_{\alpha,\,\beta})\ E_{i+1}...E_LE_1...E_{i-1}\Big)\tilde{A}^{\alpha',\beta'}_{n_i} = Tr\Big((A_{n_i}\otimes\Delta_{\alpha,\,\beta})\ G_{i+1}...G_LG_1...G_{i-1}\Big),$$

which we rewrite in short as:

$$\sum_{\alpha',\beta'} C^{\alpha,\beta,\alpha',\beta'}_{n_i}\tilde{A}^{\alpha',\beta'}_{n_i} = H^{\alpha,\beta}_{n_i}.$$

It should be noted that $\alpha,\alpha'\in\{1,...,\tilde{D}_i\}$ and $\beta,\beta'\in\{1,...,\tilde{D}_{i+1}\}$. We have thus found equation 6 in [4]. It is rather cumbersome, so we rewrite the 4'th order tensor C into a matrix and the matrices $\tilde{A}$ and H into vectors by combining the indices α',β' into a single index μ and the indices α,β into index ν. Then we obtain the sum

$$\sum_{\mu} C^{\nu,\mu}_{n_i}\tilde{A}^{\mu}_{n_i} = H^{\nu}_{n_i}, \tag{A.5}$$

or in short

$$C_{n_i}\tilde{A}_{n_i} = H_{n_i}. \tag{A.6}$$

Remember that for a system of L spins of level d, there are a total of d×L linear equations of this form that must be solved. Moreover, since C and H depend on an initial guess of $\tilde{A}$, the solutions of these equations are likely not yet optimal and performing this algorithm multiple times is advised.

B Additional Figures

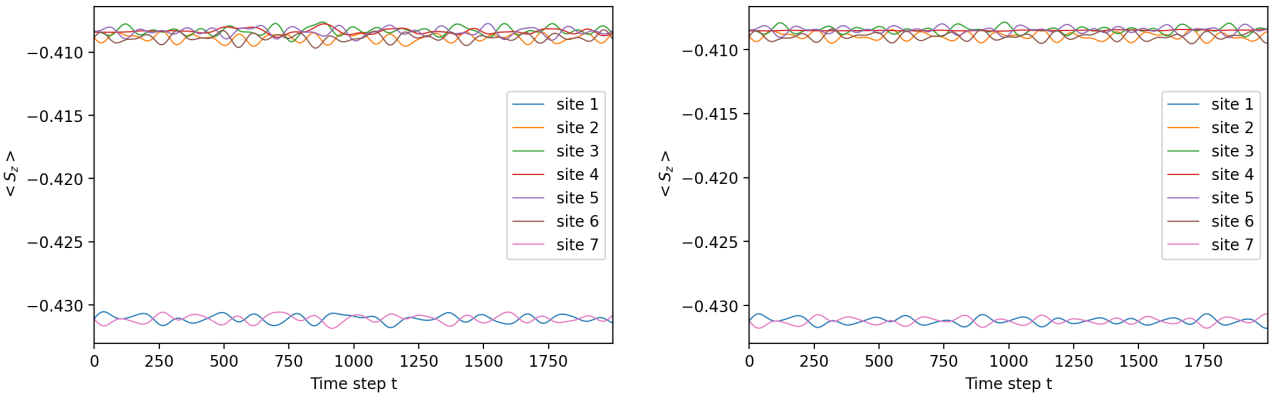

(a) $\chi = 6$ (b) $\chi = 12$

Figure B.1: At very low χ reverse time evolution of the ancilla's is not sufficient for accurate simulations.
$L = 7$, $h = 3$, $T = 2$

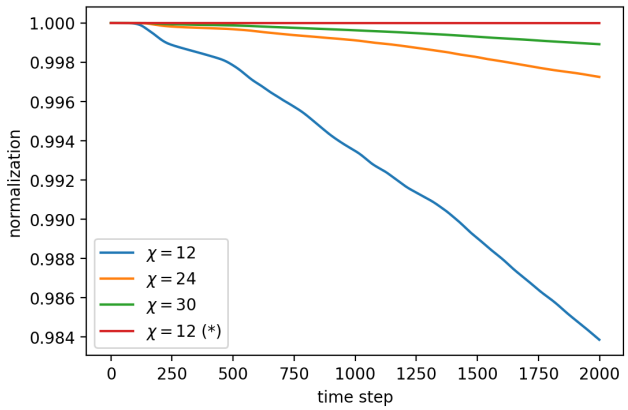

Figure B.2: Normalization of the state over real time evolution. The blue, orange and green lines are simulations where the system Hamiltonian is given by equation (31), the red line (*) is a simulation where the system Hamiltonian is that of equation (32).
$L = 7$, $h = 3$, $T = 2$

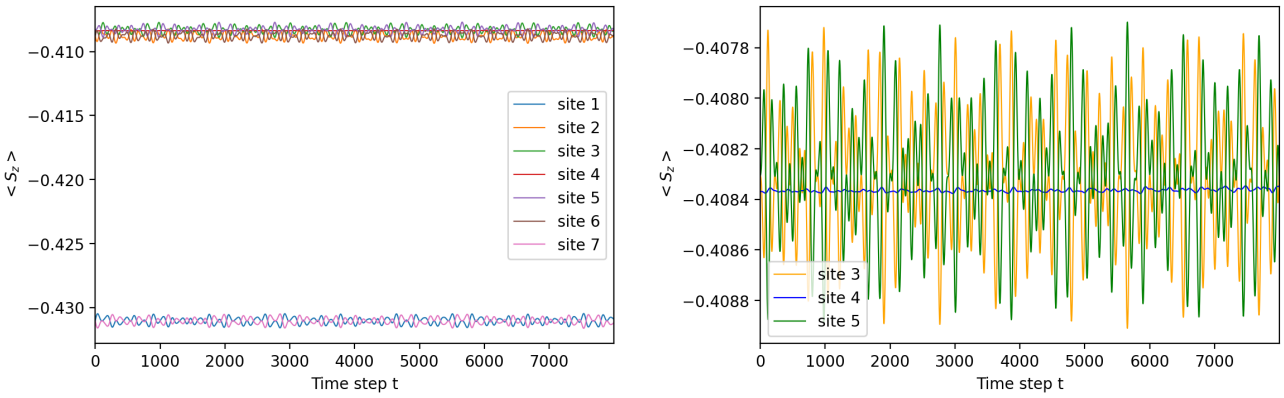

(a) (b)

Figure B.3: Simulation of a chain with $\hat{H} = \hat{H}_P \otimes \hat{\mathbb{I}} - \hat{\mathbb{I}} \otimes \hat{H}_P$ for 8000 time steps.
$L = 7$, $\chi = 24$, $h = 3$, $T = 2$

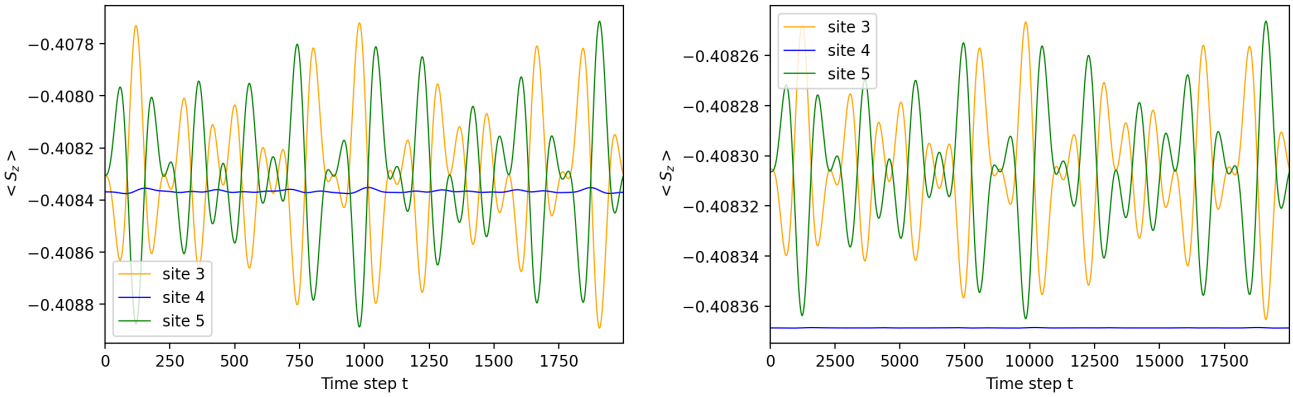

(a) time step $= 10^{-2}$ (b) time step $= 10^{-3}$

Figure B.4: Influence of the size of the time step on oscillation amplitude.
$L = 7$, $\chi = 12$, $h = 3$, $T = 2$

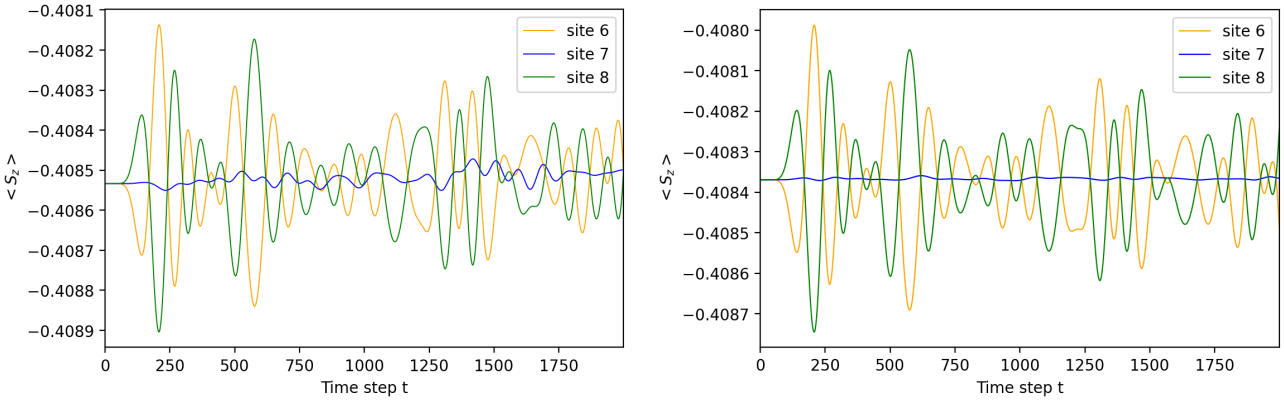

(a) $\chi = 24$ (b) $\chi = 36$

Figure B.5: Also for $\hat{H} = \hat{H}_P \otimes \hat{\mathbb{I}} - \hat{\mathbb{I}} \otimes \hat{H}_P$ a higher truncation parameter is required to simulate longer chains.
$L = 13$, $h = 3$, $T = 2$

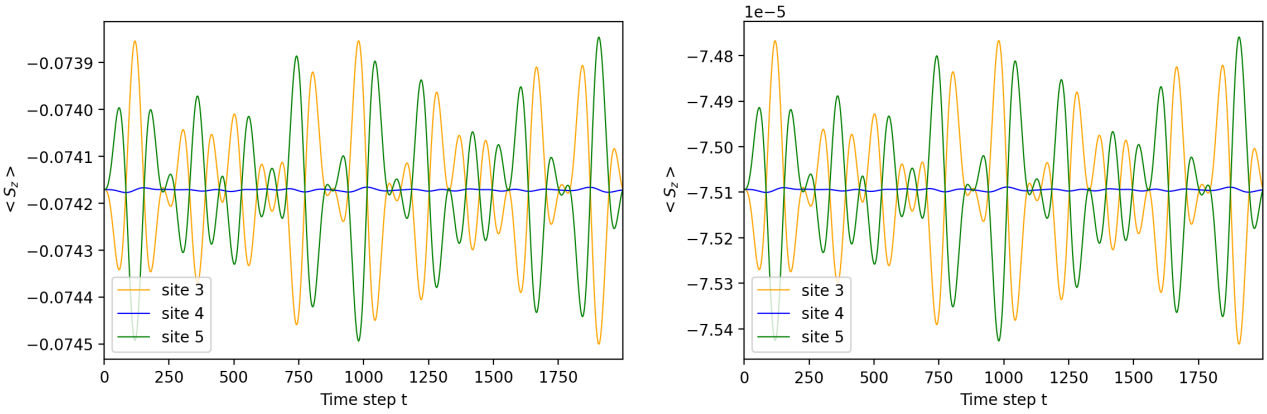

(a) $T = 20$ (b) $T = 20000$

Figure B.6: $\langle \hat{S}_z \rangle$ of the middle three sites of the chain for high temperatures.
$L = 7$, $\chi = 24$, $h = 3$

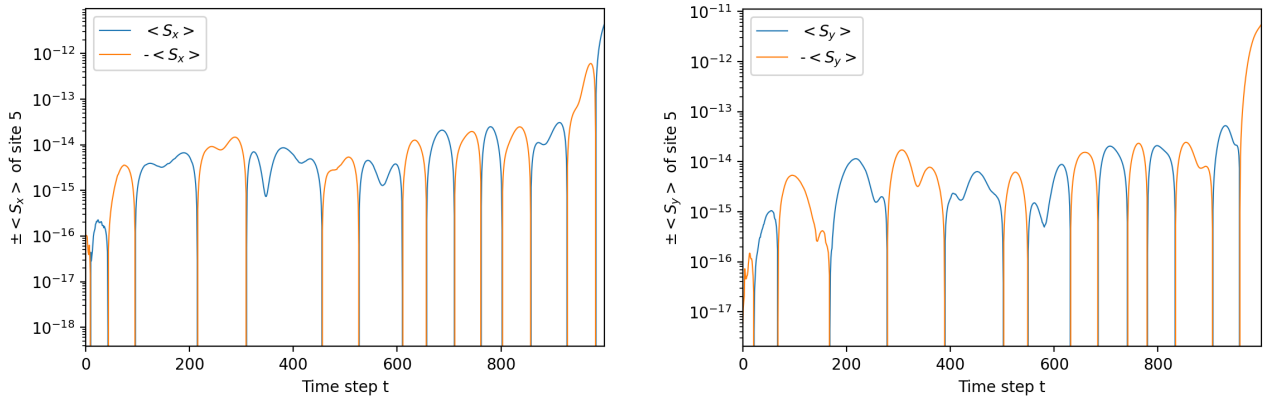

(a) (b)

Figure B.7: Log scale plots of $\langle \hat{S}_x \rangle$ and $\langle \hat{S}_y \rangle$ of the fifth site in the chain over time. Notice that this simulation is performed over 1000 time steps instead of 2000 for readability of the graphs.
$L = 7$, $\chi = 24$, $h = 3$, $T = 2$

C Python Code

The python code used for generating the results can be found in the following repository:

`https://github.com/MatthijsRepository/MPS.git`